The final publication is available at Springer via: https://link.springer.com/article/10.1007/s10518-017-0211-x

Blind prediction of in-plane & out-of-plane responses for a thin singly reinforced concrete flanged wall specimen

Farhad Dashti[1]; Rajesh P Dhakal[2]; and Stefano Pampanin[3]

Abstract This paper describes the blind prediction carried out to simulate the response of a thin reinforced concrete wall tested under uni-directional (in-plane) quasi-static reverse cyclic loading. The specimen was a singly reinforced T-shaped wall panel with a shear-span ratio of 3.7. The response of the test specimen was simulated prior to the release of test results using a finite element model which had already been verified for its capabilities in capturing different failure patterns of rectangular walls, particularly out-of-plane instability. The numerical model predicted a flexural dominated response for the specimen accompanied by considerable out-of-plane deformations. The blind prediction report, submitted in advance to the principal investigator of the experimental campaign, included lateral load-top displacement response of the specimen, maximum out-of-plane deformation corresponding to each drift level, evolution of out-of-plane displacements throughout in-plane loading, response of the longitudinal reinforcement at the section exhibiting the maximum out-of-plane deformation, and von Mises as well as reinforcement stress distribution at some key points of the wall response. Furthermore, a parametric study was carried out addressing the effects of shear-span ratio, reinforcement eccentricity and axial load ratio on the wall response. Results of the numerical simulation that had been included in the blind prediction report have been compared with the experimental measurements indicating that the evolution of the out-of-plane deformation was well captured by the model.

Keywords Reinforced concrete walls, Out-of-plane instability, Blind prediction, Parametric study

1 Introduction

Performance of structural wall systems in the 2010 Chile and the 2010-2011 Canterbury earthquakes revealed the fact that, despite having been investigated for many years, structural walls still have some

[1] PhD Candidate, Department of Civil and Natural Resources Engineering, Univ. of Canterbury, Christchurch 8140, New Zealand. E-mail: farhad.dashti@pg.canterbury.ac.nz
[2] Professor, Department of Civil and Natural Resources Engineering, Univ. of Canterbury, Christchurch 8140, New Zealand. E-mail: rajesh.dhakal@canterbury.ac.nz
[3] Professor, Department of Civil and Natural Resources Engineering, Univ. of Canterbury, Christchurch 8140, New Zealand. E-mail: stefano.pampanin@canterbury.ac.nz

issues to be solved to ensure they perform satisfactorily in relatively severe future earthquakes. Several failure patterns were observed in structural walls in these earthquakes such as buckling of bars, crushing/spalling of concrete, out-of-plane deformation also referred to lateral instability (especially involving the part of the wall length that had deteriorated in compression in previous cycles), longitudinal reinforcement failing in tension and being hidden behind a single small residual crack etc. Some of these failures are attributable to deficiencies of the associated design provisions as the requirements for confinement in the boundary element confinement or for buckling control reinforcement. However, some of the failures are not yet fully understood. In some cases, lateral instability (global buckling) of a large portion of a wall section was observed. Prior to the Chile and Canterbury earthquakes, this global buckling failure had only been primarily observed in laboratory tests (Goodsir 1985; Johnson 2010; Oesterle 1979; Thomsen IV and Wallace 2004; Vallenas et al. 1979).

In order to gain a better understanding of the seismic behaviour of structural walls, it is necessary to investigate the seismic response of walls including the causes of different failure modes observed in the recent earthquakes. As comprehensive experimental campaign at large or full scale are significantly resource-demanding, a more plausible way to scrutinize the observed performance of RC structural walls against their expected performance is to combine experimental testing and efficient numerical modelling for parametric studies, after rigorous validation and calibration on experimental data. Numerical simulation of out-of-plane buckling (also referred to as lateral or out-of-plane instability) has been seldom attempted despite it being one of the most peculiar failure patterns in the recent earthquakes in Chile and New Zealand.

Dashti et al. (2017a) (Dashti et al. 2017b) investigated the validity of a finite element modeling approach in capturing different failure mechanism of rectangular walls, with particular focus on out-of-plane instability. As a further verification, this modeling approach had been used for blind prediction of a singly reinforced wall panel tested at the Structural Laboratory of the *École Polytechnique Fédérale de Lausanne* (EPFL) (Rosso et al. 2014). A blind prediction report was submitted to the researchers in December 2014 prior to release of test results (Dashti et al. 2014). This paper presents the numerical simulation as presented in the blind prediction report as well as the comparison between the numerical and experimental results recently released and published in literature (Rosso et al. 2015).

2 Numerical model

2.1 Element Type

In this study, finite element analyses were carried out using DIANA9.4.4 (DIANA 2011). Different shell-type elements were investigated to explore their ability to accommodate the features required to

simulate the key mechanisms of wall behaviour including most of the failure modes. The curved shell elements in DIANA can be used to capture buckling and post-buckling responses based on isoparametric degenerated solid approach. Two shell behaviour hypotheses are implemented in this element (DIANA 2011): 1) Straight-normals: this hypothesis assumes that normals remain straight, but not necessarily normal to the reference surface. Transverse shear deformation is included according to the Mindlin-Reissner theory (Mindlin 1951; Reissner 1945). 2) Zero-normal-stress: it assumes that the normal stress component in the normal direction of a lamina basis is forced to zero.

In the curved shell elements, the in-plane lamina strains vary linearly in the thickness direction unlike in flat shell elements where the integration is only performed in the reference surface. This feature allows for capturing out-of-plane deformations under in-plane loading without making use of an artificial eccentricity. Three translations and two rotations are defined in every element node.

The Q20SH element, which is a four-node quadrilateral isoparametric curved shell element, is used in this study (Fig. 1a). Three-point integration scheme is considered along the thickness in which the integration points are located in the reference plane and at the two extremes of wall thickness. The integration across the thickness is performed according to the Simpson rule. Fig. 1b displays the three integration points along the thickness of a curved shell element.

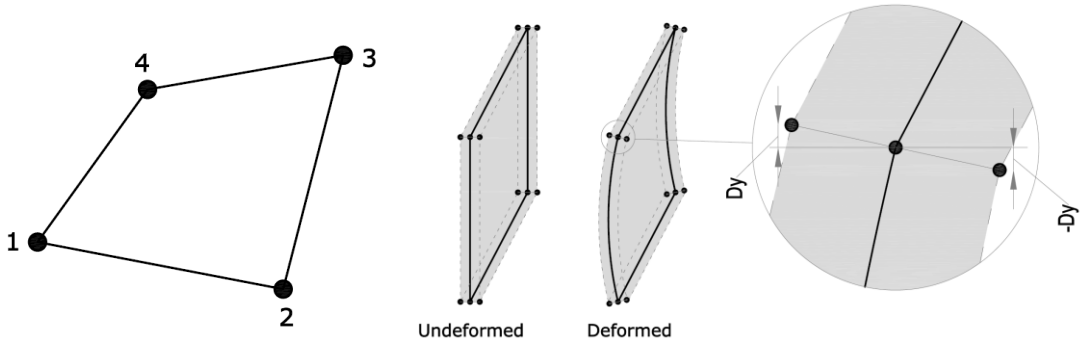

Fig. 1 Curved shell element: (a) Q20SH; (b) integration scheme across the thickness

2.2 Material Models

2.2.1 Concrete

The Total Strain Crack Model available in DIANA (DIANA 2011) is used to represent the behaviour of the concrete elements. The constitutive model based on total strain is developed along the lines of the Modified Compression Field Theory, originally proposed by Vecchio & Collins (1986). As per the multi-directional fixed crack model, the total strain based crack models follow a smeared approach for the fracture energy. A constitutive model based on total strain describes the stress as a function of the strain. In the current implementation in DIANA, the behavior in loading and unloading is modeled differently with secant (origin-centered) unloading.

During loading the concrete is subjected to both tensile and compressive stress which can result in cracking and crushing of the material. In a fixed stress-strain concept the shear behavior is modeled explicitly with a relationship between the shear stress and the shear strain. The deterioration of the material due to cracking and crushing is monitored with internal damage variables. It is assumed that damage recovery is not possible which implies that the absolute values of the internal damage variables are increasing. The loading-unloading-reloading condition is monitored with the additional unloading constraints which are determined for both tension and compression to model the stiffness degradation in tension and compression separately.

The Popovics/Mander`s constitutive model (Mander et al. 1988) (Fig. 2a) was implemented in the Total Strain Rotating Crack model to incorporate the confined concrete properties in the boundary elements. The behavior of the unconfined portion was modeled using the axial stress-strain relationship of unconfined concrete.

2.2.2 Reinforcement

The reinforcing bars are modelled using embedded reinforcement approach available in the program (DIANA 2011). In this approach, reinforcement elements are embedded in the structural elements, referred to as mother elements. DIANA ignores the space occupied by the embedded reinforcing bars; the mother element neither diminishes in stiffness, nor in weight (mass). The reinforcement does not contribute to the weight (mass) of the element. Standard reinforcement elements do not have degrees of freedom of their own. In standard reinforcement, the strains are computed from the displacement field of the mother elements. This implies perfect bond conditions between the reinforcement and the surrounding concrete. The stress-strain curve of the reinforcing steel is defined using Menegotto and Pinto (1973) model (Fig. 2b). The modification proposed by Filippou et al. (1983) is implemented to allow for the effects of isotropic strain-hardening. Bar buckling is not included in this constitutive model, hence the effect of bar buckling is neglected in the analysis conducted in this paper.

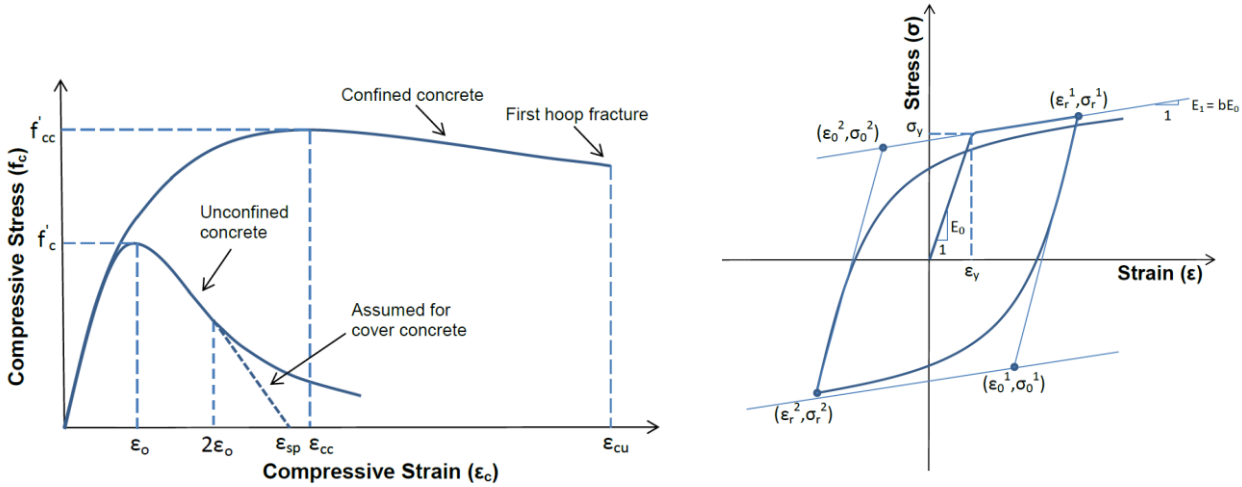

(a) Concrete (Mander et al. 1988)

(b) Steel (Menegotto and Pinto 1973)

Fig. 2 Constitutive models of materials

3 Blind predictions

Dimensions and reinforcement layout of the test specimen are shown in Fig. 3. The specimen was tested at full scale and the dimensions and reinforcement details followed current design practices for low- to mid-rise construction of residential buildings in Colombia representing a shear-span ratio of 3.7. The specimen was 80 mm thick, 2700 mm long and 2000 mm tall. Height of the wall in the actual building was 2200, but due to laboratory space constraints, the specimen height was reduced to 2000 mm. The specimen had a shear span of 10m and represented a portion of a multi-storey wall. This shear span was provided by the loading pattern. The specimen had a flange at the north end that was 80 mm thick and 440 mm long to replicate the effect of a perpendicular wall on member stability. According to the CAD file provided by the experimenters, the longitudinal reinforcement was positioned with an eccentricity with respect to the section centreline as shown in Fig. 4. The effect of this eccentricity on the predicted results will be discussed afterwards.

According to the test report, the wall was subjected to lateral displacement cycles in accordance with the drift history shown in Fig. 5. Two vertical actuators were used to apply an axial load ratio $\nu=N/(f'cAc)$ =0.05 as well as the bending moment corresponding to the shear span of 10m (shear-span ratio of 3.7). In order to ensure that the shear span of 10m was maintained during the analysis, the displacement was applied at a higher elevation through an elastic extension so that the total effective height of the wall could be 10m. As the displacement was measured at the height of the actuator (2.2 m from the base) in the test, the ratio between the analytically applied displacement at the elevation of 10m to the displacement at the actuator elevation was captured at different stages of wall nonlinear response using a monotonic push-over analysis.

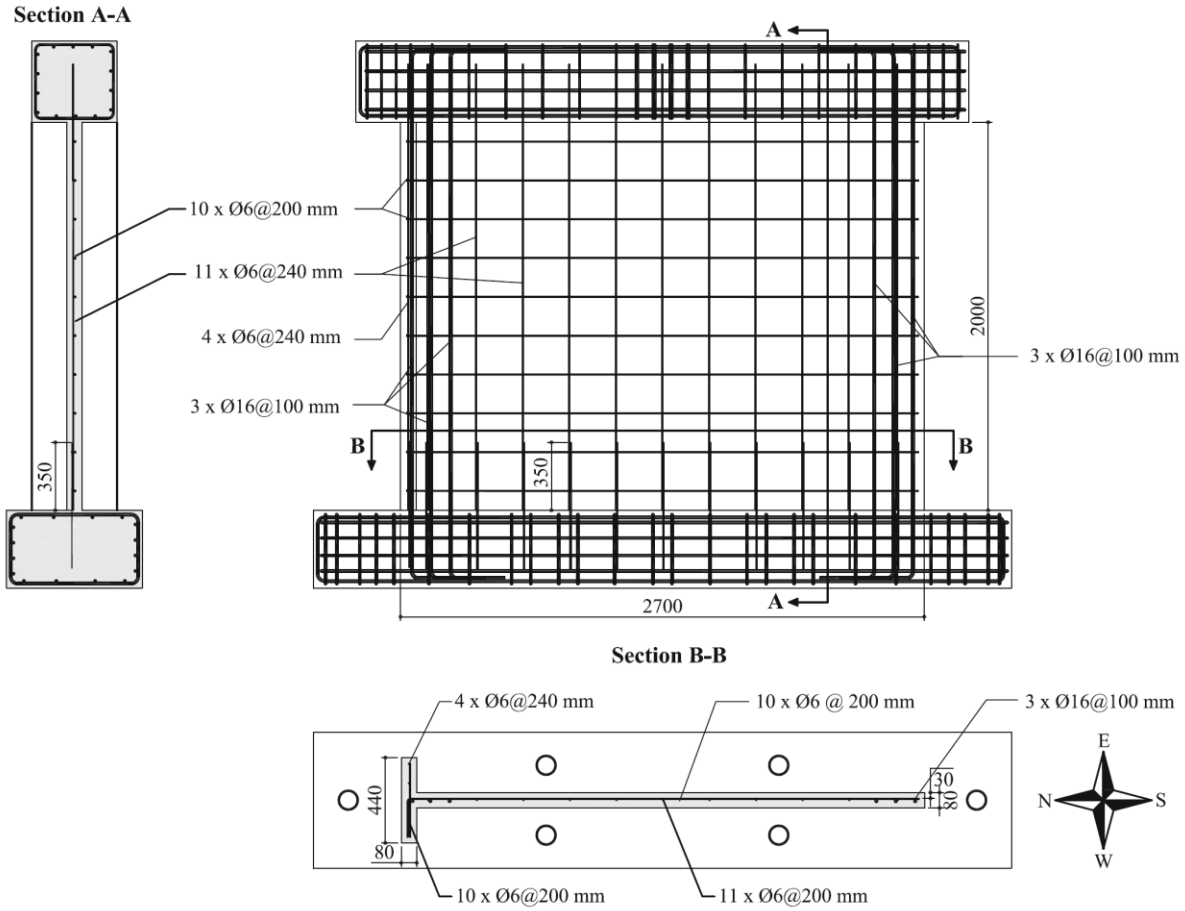

Fig. 3 Dimensions and reinforcement layout of the test specimen (Rosso et al. 2015)

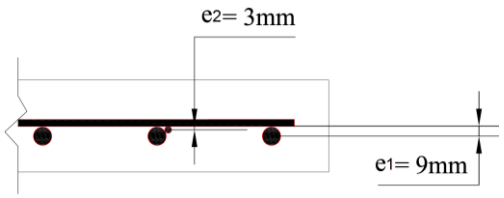

Fig. 4 Eccentricities of the longitudinal reinforcement

Fig. 6 shows a schematic view of the finite element model with loading and boundary conditions. The specimen was restrained against out-of-plane displacements at the storey height using steel tubes to prevent the top RC beam from moving sideways. The constraint system adopted in the experiment to restrain the out-of-plane displacement at the cap beam level and its representation in the numerical model is shown in Fig. 6b. The wall section was modelled using the curved shell element, with a larger thickness in the flange part. The difference in shell thickness is shown using the extruded view (Fig. 6c). Mesh sensitivity analysis was not carried out and a relatively fine mesh was adopted to capture a better prediction of the wall height undergoing the maximum out-of-plane displacements.

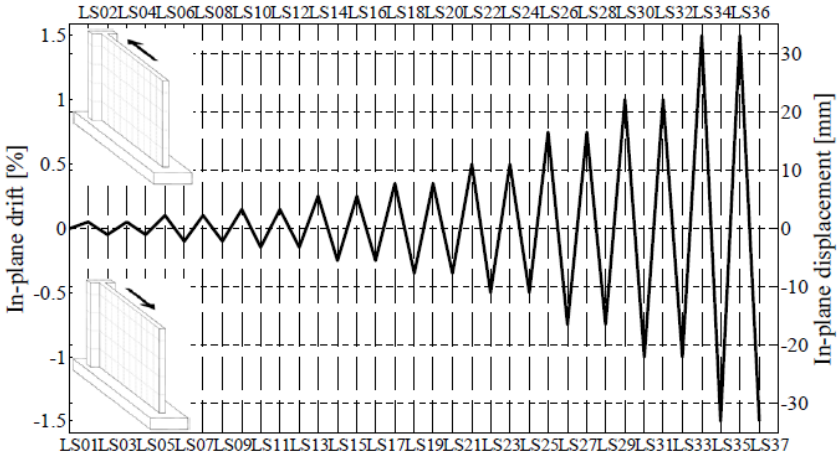

Fig. 5 Applied drift history throughout load stages (Rosso et al. 2014)

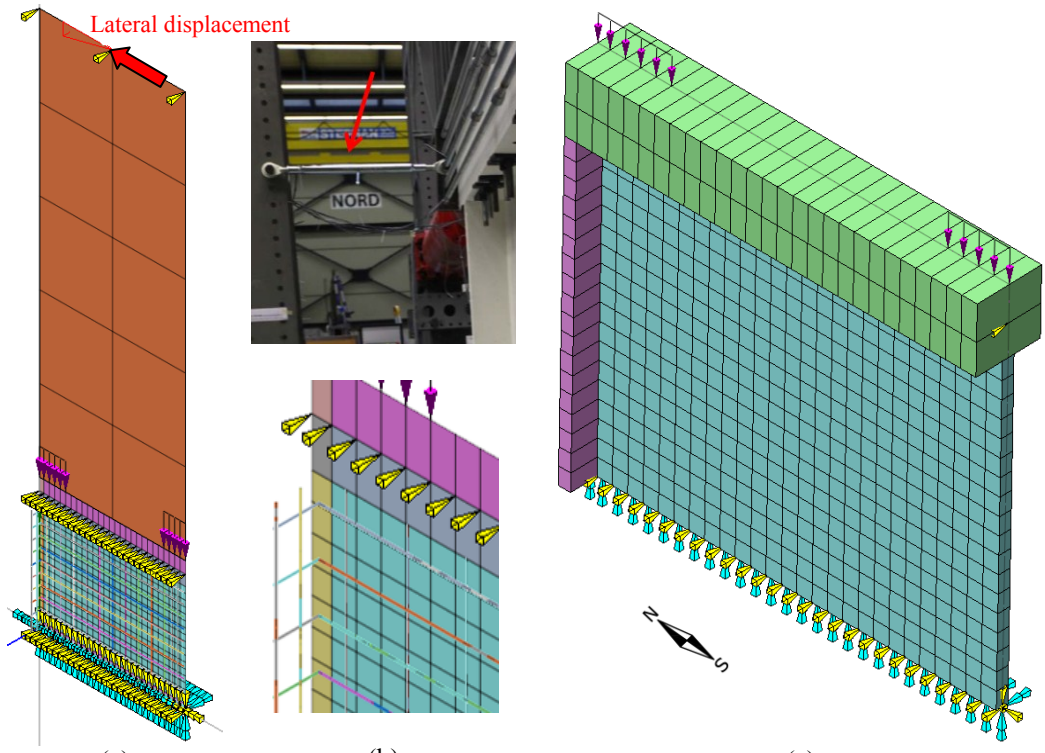

(a) (b) (c)

Fig. 6 Finite element model: (a) increased height of the lateral load to generate the shear span of 10m; (b) experimental vs numerical model restraint against out-of-plane displacement at cap beam level, photo courtesy of Rosso et al. (2014); (c) extruded 3-D view of the model

Several parameters are known to influence the out-of-plane instability of rectangular walls, such as wall thickness, axial load ratio, etc. The effects of some of these parameters are investigated in this study. Table 1 displays the set of wall models analyzed in this study with the parameters changing in each model. Models TW1-A to TW1-D comply with the test shear-span ratio. Eccentricity and axial load ratio are the parameters changing in this set of models. As noted above, the specimen had an eccentricity in positioning of the longitudinal reinforcement. As a part of parametric investigation, this

eccentricity was neglected in some models and the axial load ratio of 0.05 applied in the test was also dropped to 0.0 in some models.

In order to evaluate the relationship between out-of-plane deformations and the shear-span ratio, which determines whether the wall response will be flexure or shear-dominated, the models TW1-A to TW1-D were subjected to a loading corresponding to a very low shear-span ratio of 0.8, compared to the axial load ratio of 3.7 that was adopted in the test .

These cases are denoted as TW1-a to TW1-d, respectively (Table 1). For this purpose, the lateral displacement was applied at the same elevation as the test actuator so that the effect of additional moment applied through vertical actuators would be eliminated. This loading condition, shown in Fig. 7, represents a shear-span ratio of 0.8 which is considerably smaller than that of the benchmark test TW1-A, and can significantly change the wall response.

Table 1 Cases considered for sensitivity analysis

	Model	Shear-span ratio	Eccentricity	Axial load ratio
1	TW1- A (Test Specimen)	3.7	Yes	0.05
2	TW1- B	3.7	Yes	0.00
3	TW1- C	3.7	No	0.05
4	TW1- D	3.7	No	0.00
5	TW1- a	0.8	Yes	0.05
6	TW1- b	0.8	Yes	0.00
7	TW1- c	0.8	No	0.05
8	TW1- d	0.8	No	0.00

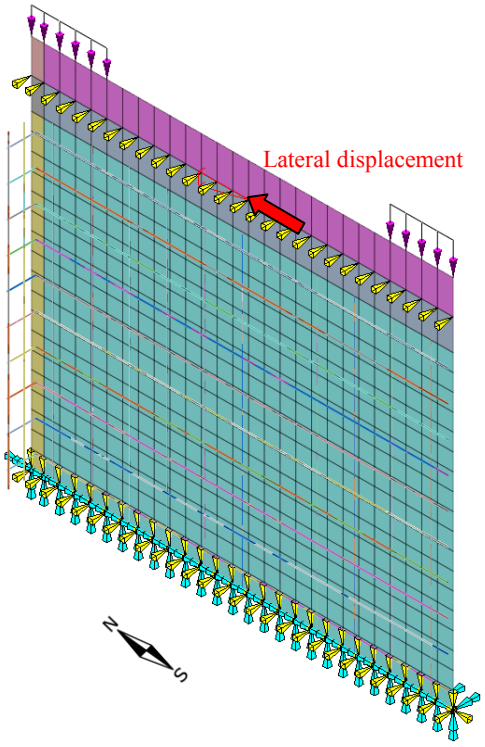

Fig. 7 Model with a low shear-span ratio

3.1 TW1-A (Test Specimen)

The longitudinal reinforcement eccentricity was considered in this model, and the axial load was applied according to the test program. The predicted response of this specimen was governed by flexural deformations and was accompanied by out-of-plane deformations in the south boundary zone. The flange part of the wall section, as expected, did not exhibit out-of-plane deformations. Fig. 8 displays the lateral load versus top displacement response of the specimen as well as the maximum out-of-plane displacement at each drift level. The key points corresponding to degradation of the model are displayed in this figure. At Point a, the maximum compression strength in the concrete was achieved at the base section in the flange. Fig. 9 displays the von Mises stress distribution of the model at this point showing the concentration of stress at the compression toe. As there was no confinement provided along the wall section, the compressive stress carrying capacity of the concrete dropped considerably at this point resulting in the degradation of the lateral load observed at Point a. At Point b, as shown in Fig. 10, the longitudinal reinforcement in the compression zone has gone through considerable yielding. At this point, the wall had elongated due to residual strain of the reinforcement, which prevented the cracked concrete from closing fully and the majority of the load carrying capacity was provided by the reinforcement in compression. At Point c, a very significant degradation coming from the out-of-plane instability of the south (i.e. opposite to the flange) boundary zone is observed. As shown in Fig. 8b, the out-of-plane deformation starts during the 0.5% drift cycle, gradually increases at the 0.75% and 1% drift cycles, and results in a sudden out-of-plane instability at 1.5% drift level. Fig. 8a shows the considerable degradation of the model at Point c when reversing from +1.5% drift to -1.5% drift. At this point, the south boundary zone, which had experienced a large tensile strain at +1.5% drift, is gradually subjected to compressive stress; thereby causing a considerable out-of-plane deformation.

Fig. 11a indicates the maximum out-of-plane deformation of the model during 1.5% drift level and Fig. 11b displays the maximum out-of-plane displacement at the south boundary zone at different stages of loading. As shown in this figure, at 0.5%, 0.75% and 1.0% drift levels, the out-of-plane deformation increases when reversing from peak positive drifts, and decreases when reaching the peak negative drifts, which is the general trend of this mode of deformation (Beattie 2004; Chai and Elayer 1999) before it results in the wall instability. After reaching the 1.5% drift cycle, the out-of-plane deformation does not recover during the drift reversals and results in response degradation of the model.

It is worth noting that the displacement in the numerical simulation was controlled at the top of the 10m high model (Fig. 6a) whereas in the experiment the displacement was applied at the actuator level located at 2.2 m height. As a result, at different levels of material nonlinearity, the displacement at the top of the numerical model was amplified when compared to the corresponding target displacement at the actuator level. However, due to the out-of-plane instability, the displacement at

the top of the model increased significantly and reached the predefined target before the displacement at the actuator level would reach the desired drift level. Therefore, the displacement at the actuator level, which is indicated as “Top Displacement” in the figures, could not reach the experimentally applied -1.5% drift.

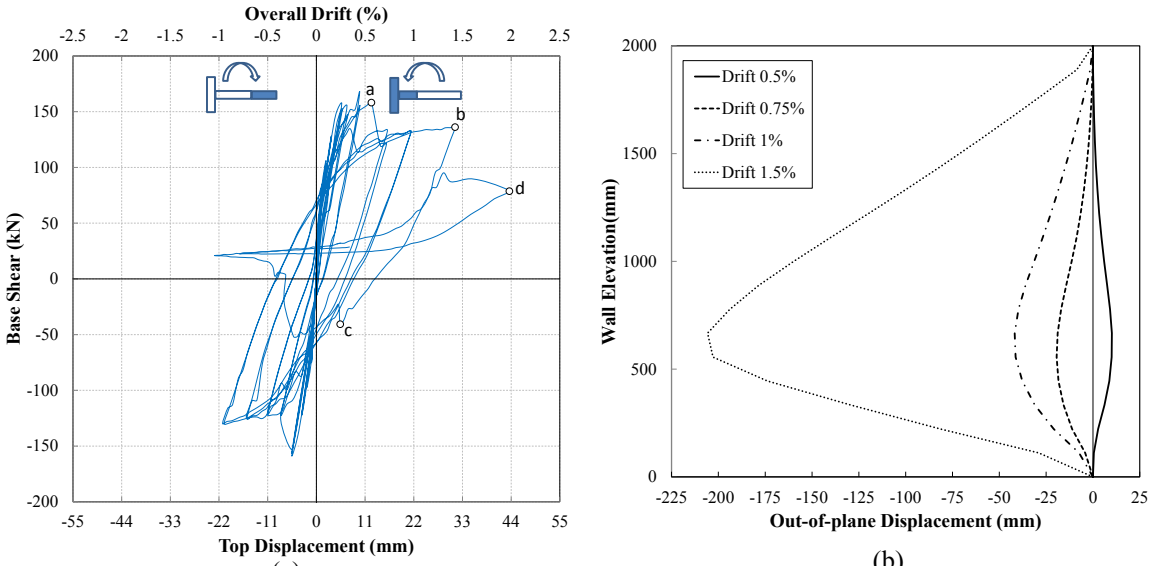

(a) (b)

Fig. 8 Model response, TW1- A: (a) lateral load vs top displacement response; (b) maximum out-of-plane deformation corresponding to each drift level

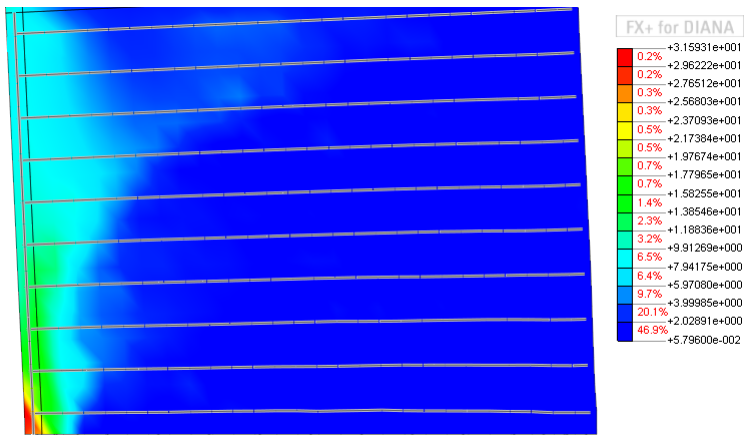

Fig. 9 Von Mises stress distribution, TW1-A, Point a

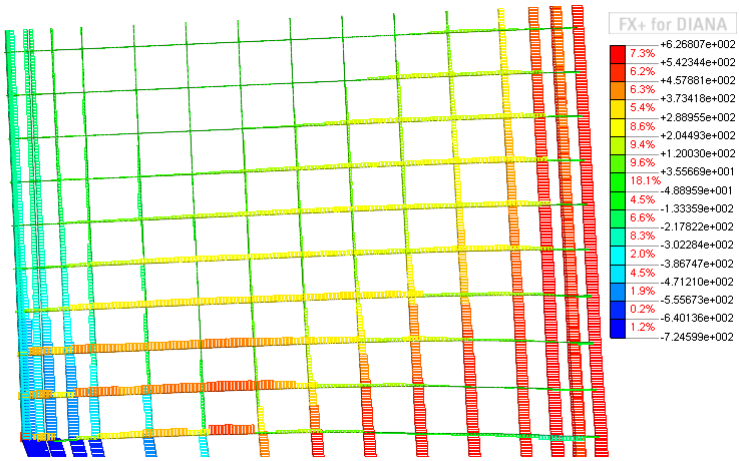

Fig. 10 Reinforcement stress, TW1-A, Point b

At Point d, the shear resistance of concrete is degraded, the von Mises stress distribution (Fig. 12) and the reinforcement stress (Fig. 13) show that the concrete is mostly unable to sustain more than 6 MPa of stress throughout the wall length, and the three lowest layers of horizontal reinforcement elements have crossed their yield limit. Interesting to note that this effect was not observed in the monotonic pushover curve, compared in Fig. 14 with the cyclic hysteretic response; this difference is expected as the shear resistance of concrete is known to degrade during cyclic loading with increasing ductility demands (Krolicki et al. 2011).

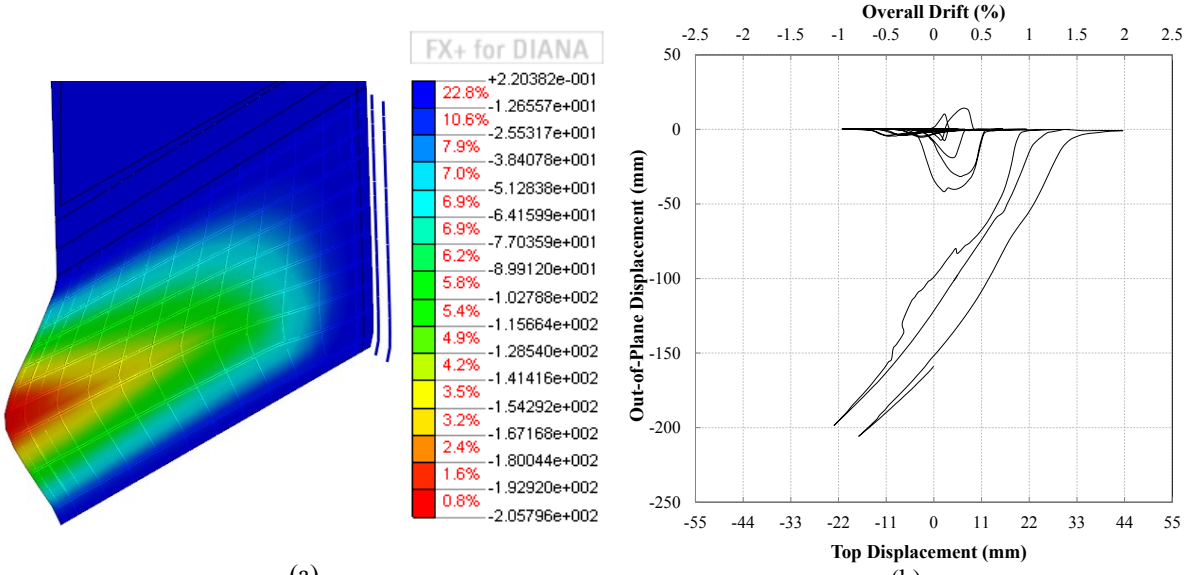

(a) (b)

Fig. 11 Out-of-plane deformation-TW1-A: (a) deformation pattern at 1.5% drift cycle; (b) maximum out-of-plane displacement throughout the loading

The out-of-plane deformation is typically localised within the end regions of the wall (as shown in Fig. 11a) where vertical tensile and compressive strains from the in-plane cyclic actions are greatest, and the considerable residual strain of the reinforcement does not allow for crack closure before the

reinforcement yielding in compression results in out-of-plane instability of the wall (Chai and Elayer 1999; Paulay and Priestley 1993).

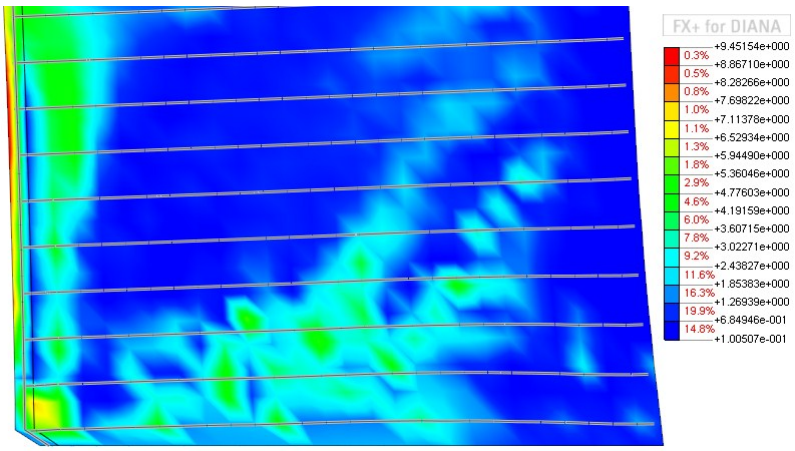

Fig. 12 Von Mises stress distribution, TW1-A, Point d

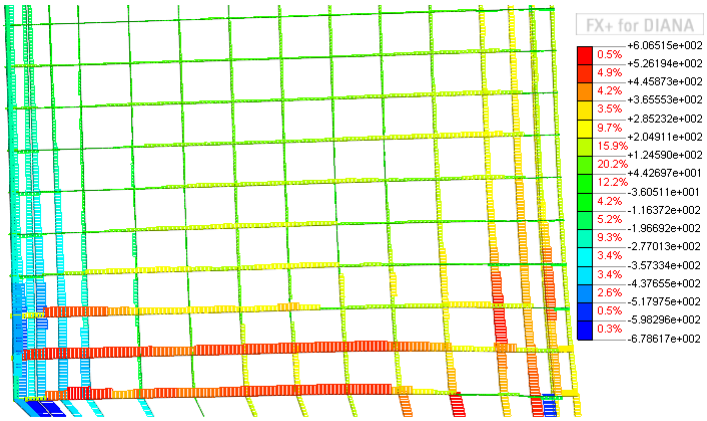

Fig. 13 Reinforcement stress, TW1-A, Point d

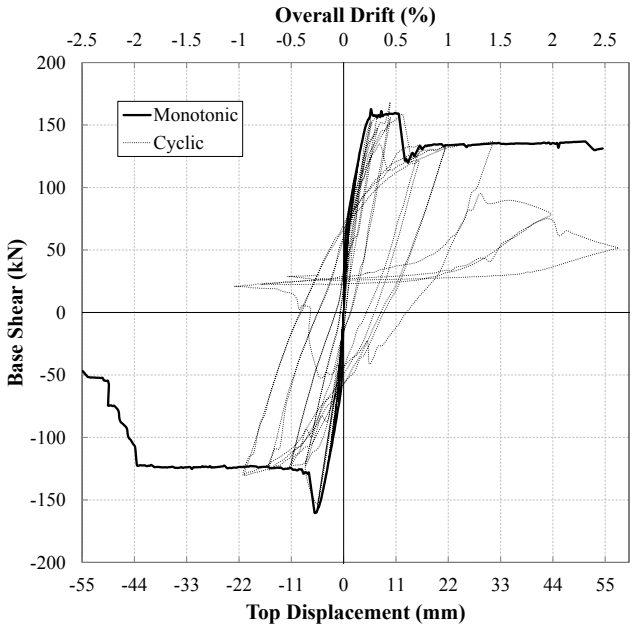

Fig. 14 Comparison of monotonic and cyclic response of TW1-A

The strain history of the reinforcement at the end region of the wall corresponding to the section exhibiting the maximum out-of-plane deformation is plotted in Fig. 15. As can be noted, the reinforcement strain increases along with the increase of the top lateral displacement and the residual strain accumulates as a result of cyclic loading. Fig. 15a shows that the maximum strain reached by the reinforcement prior to the abrupt increase of the out of plane deformation was ε_{sm}= 0.0204. The level of tensile strain reached by the end region reinforcement at each cycle is in fact acknowledged to be one of the most significant parameters governing the probability of out-of-plane instability when this reinforcement is subjected to compression (Chai and Elayer 1999; Moyer and Kowalsky 2003; Paulay and Priestley 1993).

Fig. 15a and Fig. 15b display the residual strain and wall elongation developed throughout the loading history. It can be noted that even under axial load ratio of 0.05, the strain at this region of the wall is mostly tensile throughout the loading, confirming that the axial load carrying capacity at this region is provided by the reinforcement only. In such conditions, small levels of eccentricity of the longitudinal reinforcement can easily trigger the out-of-plane instability of the wall.

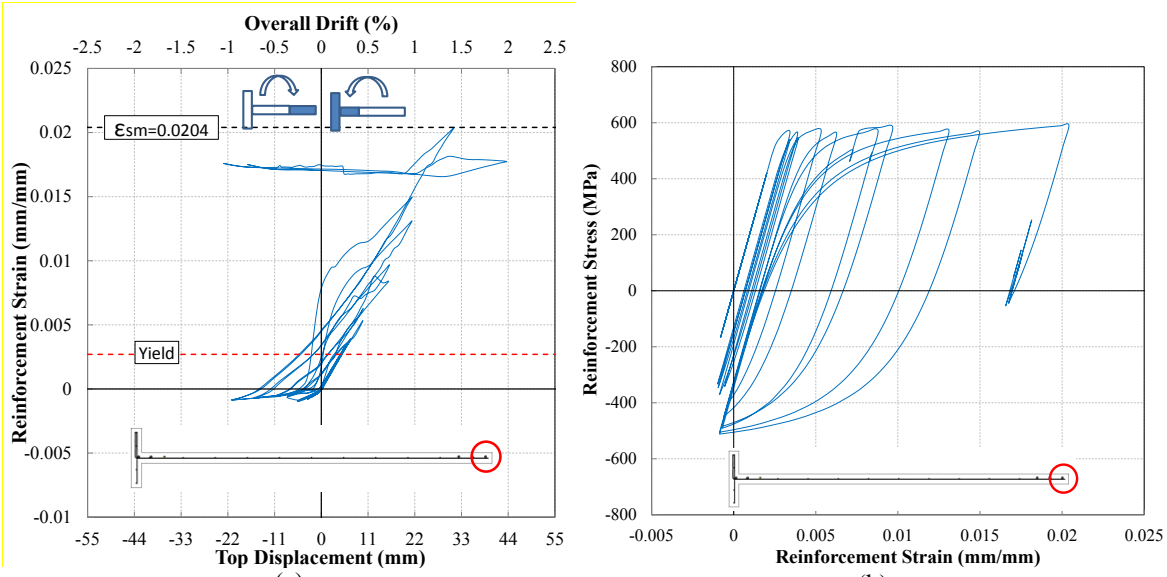

Fig. 15 Response of the longitudinal reinforcement at the section exhibiting maximum out-of-plane deformation, TW1- A: (a) strain history; (b) stress-strain curve

3.2 TW1- B

In order to investigate the effect of axial load ratio on the response of the wall, the previous model was analysed without any axial load. The numerical model response (Fig. 16) shows that although this model did not exhibit the strength degradations observed at Points a, b and d in TW1-A (see Fig. 8), the removal of the axial load did not prevent the out-of-plane deformation of the south boundary zone which started at the same drift level as in TW1-A. In fact the out-of-plane displacement in this model at 1% drift is considerably larger than that in TW1-A. Fig. 16a displays the considerable degradation

associated with the out-of-plane instability of the model. The development of the out-of-plane displacement at different stages of loading (Fig. 17) shows the same trend as TW1-A. Fig. 18 shows the strain history of the longitudinal reinforcement at the section exhibiting maximum out-of-plane deformation. The comparison between this figure and Fig. 15 helps understanding the effect of axial load on the residual tensile strain developed in the reinforcement, which in turns results in the elongation of the wall. The removal of the axial load resulted in out-of-plan instability of the model at 1% drift when the end reinforcement had already experienced a strain of ε_{sm}= 0.0169. The reinforcement strain at this drift level was 0.015 in TW1-A.

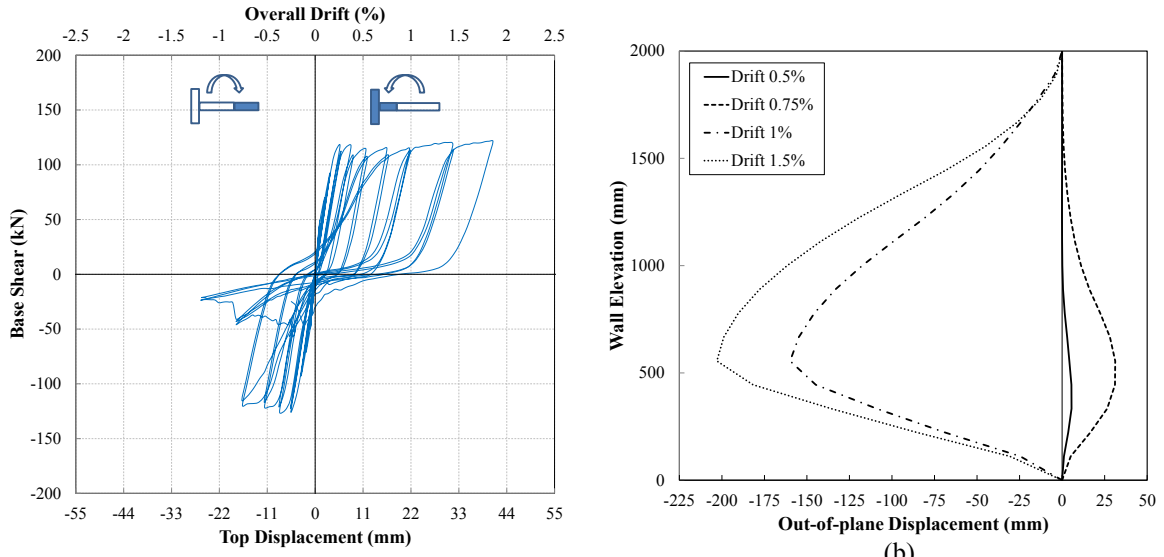

Fig. 16 Model response, TW1- B: (a) lateral load vs top displacement response; (b) maximum out-of-plane deformation corresponding to each drift level

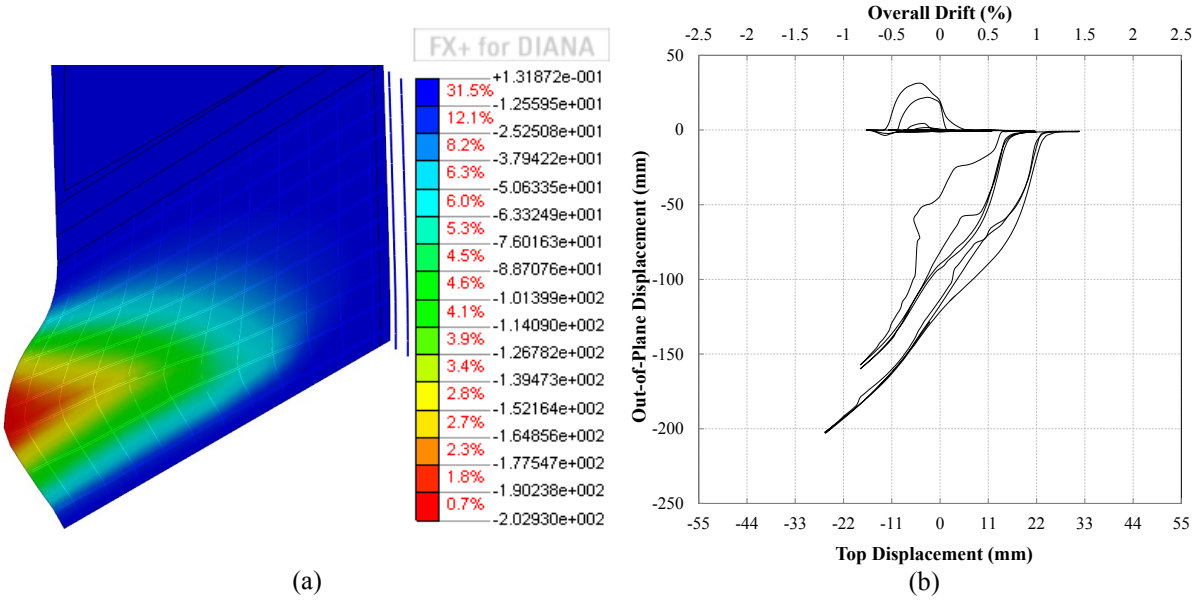

Fig. 17 Out-of-plane deformation-TW1-B: (a) deformation pattern at 1.5% drift cycle; (b) maximum out-of-plane displacement throughout the loading

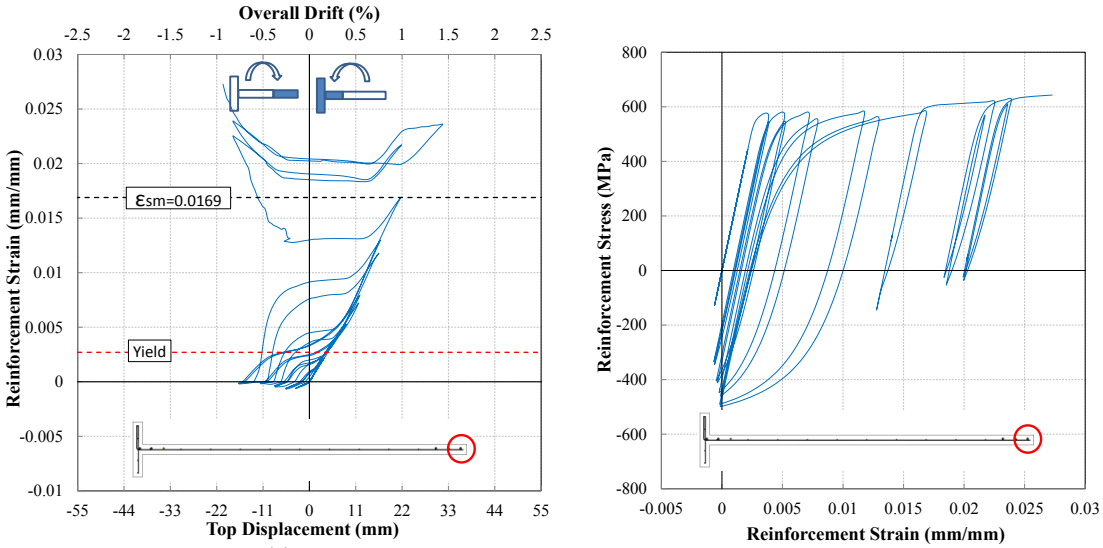

Fig. 18 Response of the longitudinal reinforcement at the section exhibiting maximum out-of-plane deformation, TW1- B: (a) strain history; (b) stress-strain curve

3.3 TW1- C

In this section, the effect of reinforcement eccentricity on development of the out-of-plane deformation is evaluated. For this purpose, the longitudinal and horizontal reinforcement elements are positioned at the section centreline with no eccentricity. The results shown in Fig. 19 to Fig. 21 show that the eccentricity does not play a significant role in preventing or triggering the out-of-plane instability of this model as the difference between the results of the model with eccentricity (TW1-A) and the model without eccentricity (TW1-C) is negligible. It should be noted that the analysis results for the benchmark model with eccentricity showed very small out-of-plane deformations starting from the loading initiation, whereas the out-of-plane deformation of the model without eccentricity was zero up to a certain level (0.75% drift level).

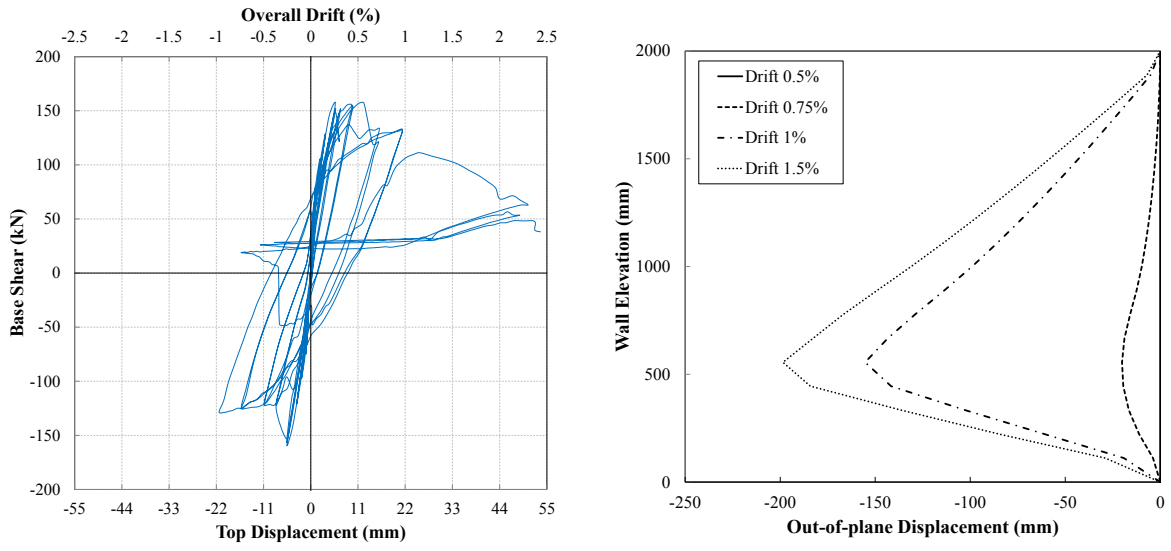

Fig. 19 Model response, TW1- C: (a) lateral load vs top displacement response; (b) maximum out-of-plane deformation corresponding to each drift level

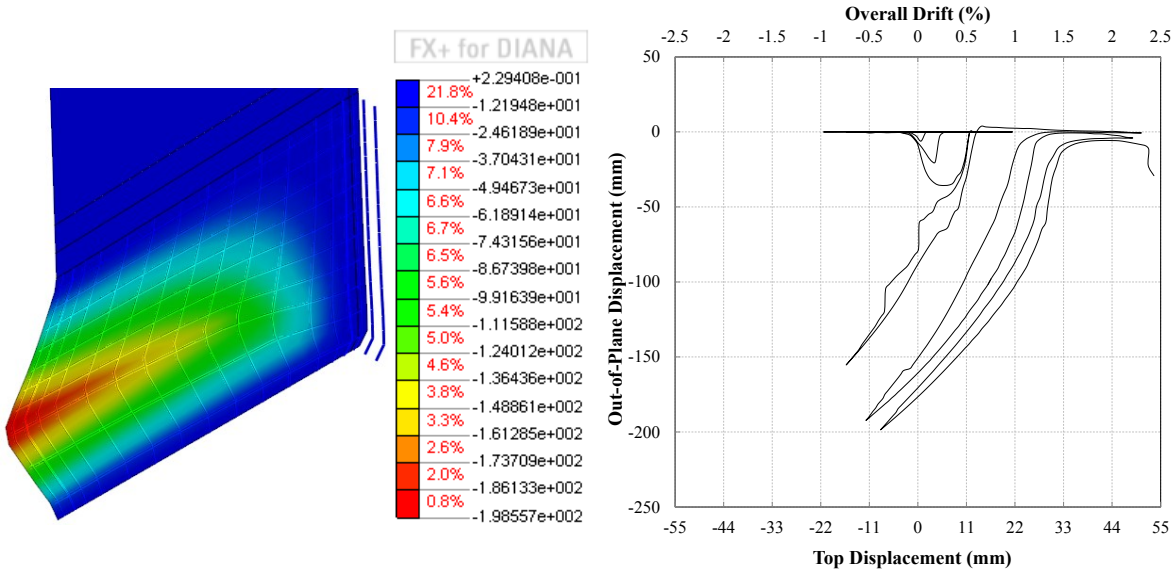

(a) (b)

Fig. 20 Out-of-plane deformation-TW1-C: (a) deformation pattern at 1.5% drift cycle; (b) maximum out-of-plane displacement throughout the loading

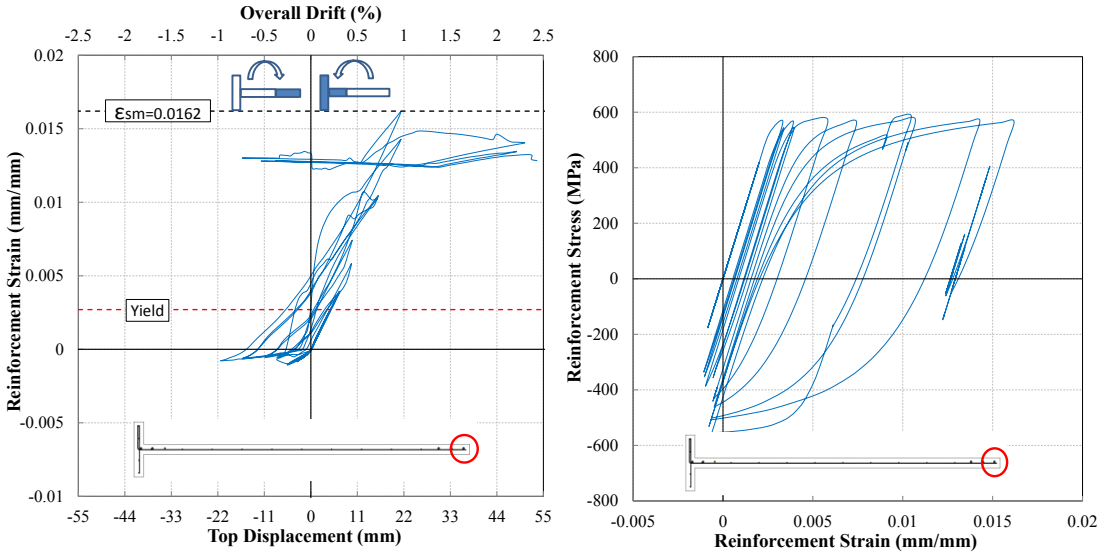

(a) (b)

Fig. 21 Response of the longitudinal reinforcement at the section exhibiting maximum out-of-plane deformation, TW1- C: (a) strain history; (b) stress-strain curve

3.4 TW1- D

The model without eccentricity is analyzed with also zero axial load ratio to evaluate the effect of axial load ratio on response of the concentrically loaded wall. The results of this model TW1-D (Fig. 22 to Fig. 24) do not indicate a considerable difference with respect to the model with eccentricity and no axial load (TW1-B).

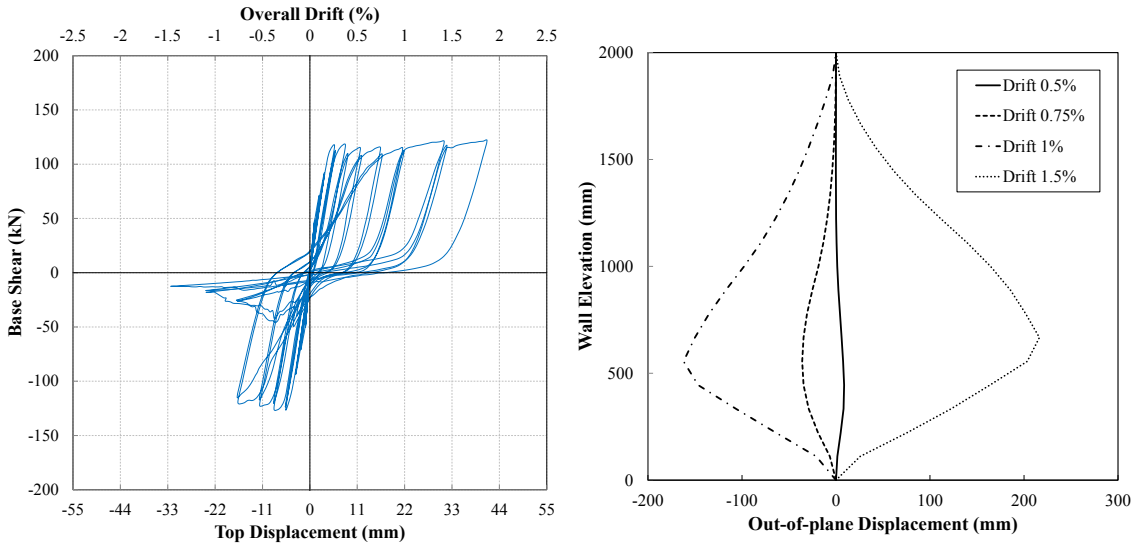

(a) (b)

Fig. 22 Model response, TW1- D: (a) lateral load vs top displacement response; (b) maximum out-of-plane deformation corresponding to each drift level

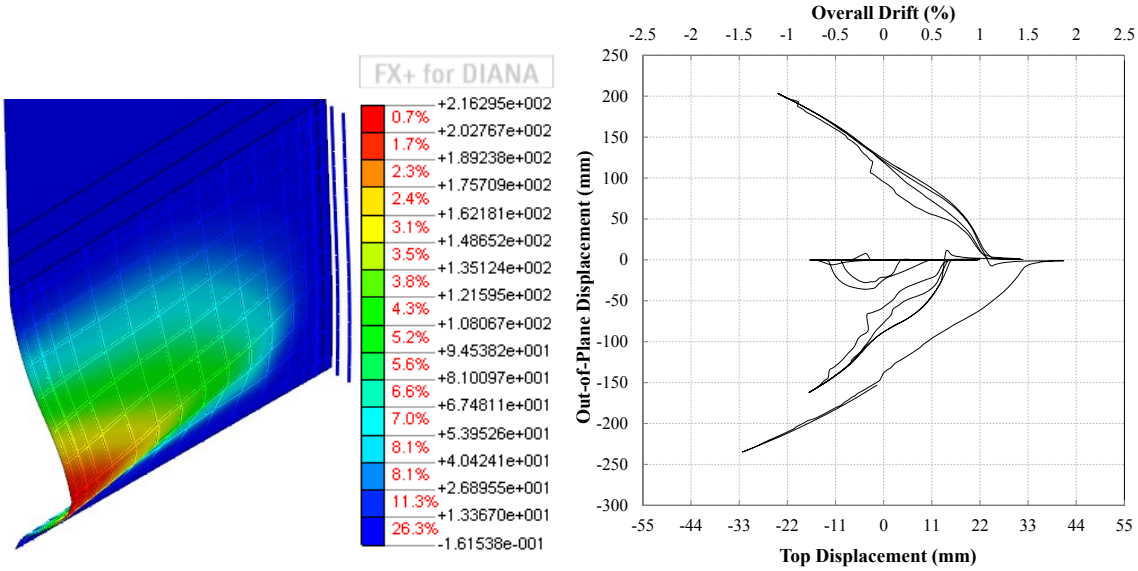

(a) (b)

Fig. 23 Out-of-plane deformation-TW1-D: (a) deformation pattern at 1.5% drift cycle; (b) maximum out-of-plane displacement throughout the loading

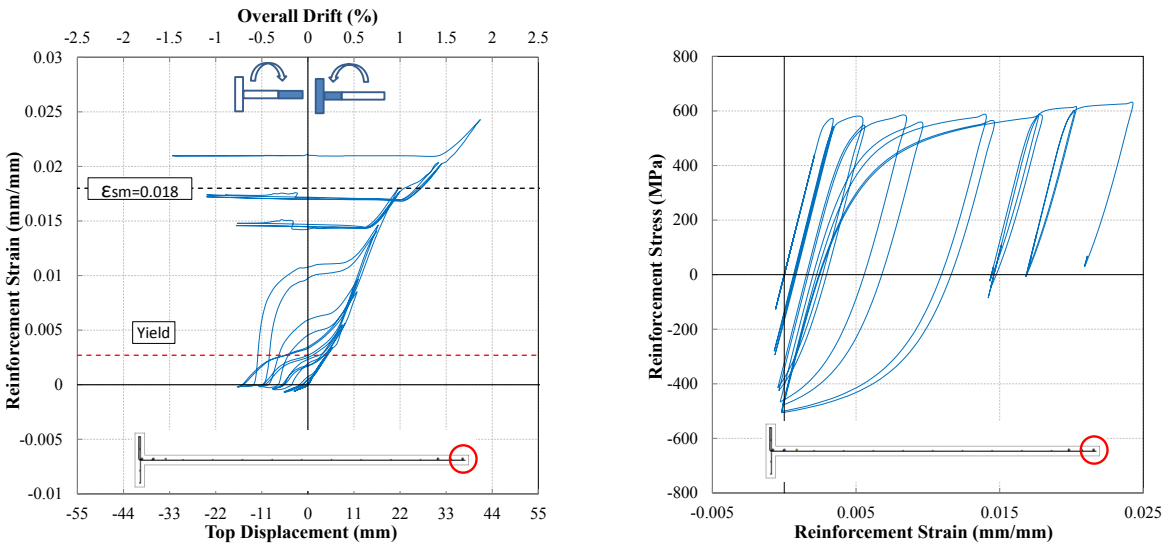

(a) (b)

Fig. 24 Response of the longitudinal reinforcement at the section exhibiting maximum out-of-plane deformation, TW1- D: (a) strain history; (b) stress-strain curve

3.5 TW1-a

In the model TW1-a, the reinforcement eccentricity was considered, and the axial load was applied according to the test program. The model differs from the benchmark test specimen TW1-A only for the shear span ration, reduced from 3.7 to 0.8 to investigate the effect of shear dominated response to the development of out-of-plane mechanism. The response of this specimen was, as expected, governed by shear deformations and was accompanied by a limited out-of-plane deformation at the south boundary zone. The flange part of the wall section, as expected, did not exhibit out-of-plane deformation. Fig. 25 displays the lateral load versus top displacement response of the specimen as well as the maximum out-of-plane displacement at each drift level. As shown in Fig. 25a, combination of the axial load and the wall geometry (i.e. squat wall) resulted in the shear dominated response of the wall. Fig. 8b shows development of the out-of-plane displacement starting from 0.5% drift level and increasing considerably at 1% and 1.5% drift levels. The out-of-plane displacement is minor in this case, only about 5% of that observed in TW1-A (e.g. max of 6 mm at 1.5% drift in TW1-a compared to 200 mm at 1.5% drift in TW1-A).

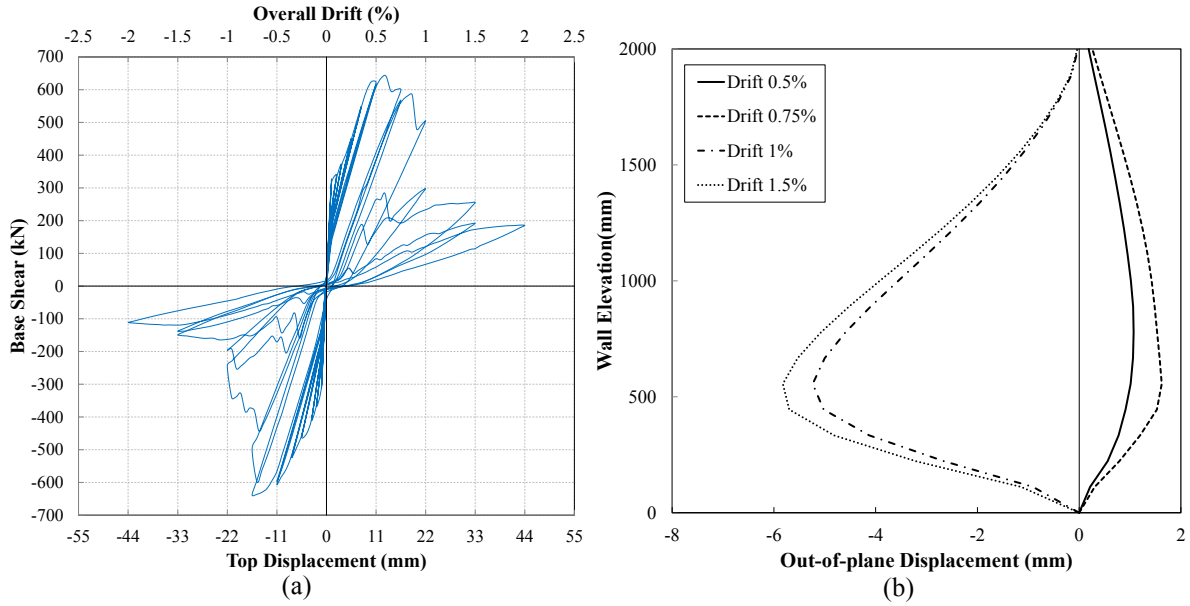

Fig. 25 Model response, TW1-a: (a) lateral load vs top displacement response; (b) maximum out-of-plane deformation corresponding to each drift level

Fig. 26a indicates the von Mises stress distribution of the model at 1.5% drift level when the out-of-plane displacement is developed at the south boundary zone, as shown in Fig. 26b. The von Mises stress distribution shows development of the diagonal strut action with some partial vertical compression struts (mainly due to the axial load), and the dark blue region shows the area damaged considerably. As no load is carried by this area, the von Mises stress is understandably close to zero. The vertical strut at the boundary region is in fact not developed in the outer face of the section undergoing out-of-plane deformation, which has a von Mises stress value close to zero. On the other hand, the inner face of the section undergoing out-of-plane deformation (not presented herein), being under further compression, forms a strut and transfers the axial force to the base.

The strain history of the reinforcement at the end region of the wall corresponding to the section exhibiting the maximum out-of-plane deformation is plotted in Fig. 27. It can be noted that up to 1% drift, there is an increase in the reinforcement strain along with increase of the top displacement and accumulation of residual strain as a result of cyclic loading. After that level of drift, there is a considerable decrease in the reinforcement strain which can be attributed to the shear failure of the model as a result of wall geometry and axial load ratio. The difference in this regard between this case and the corresponding model with high shear-span ratio (TW1-A, Fig. 15a) is quite noticeable.

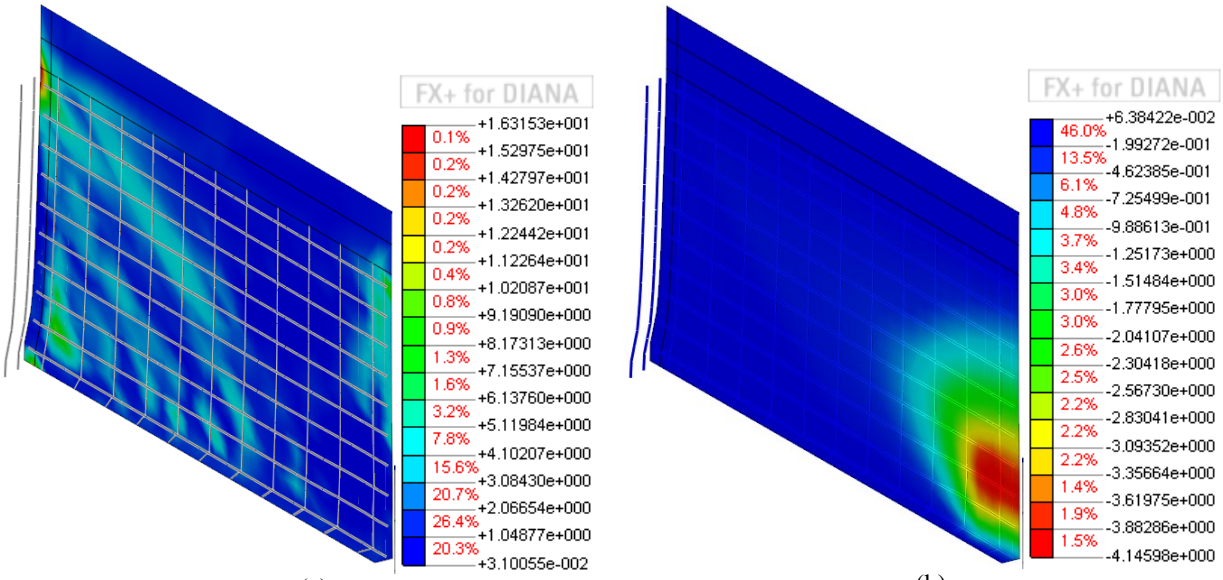

(a) (b)

Fig. 26 Model response at -1.5% drift, TW1-a: (a) von Mises stress distribution; (b) out-of-plane deformation

Fig. 27a and Fig. 27b display the residual strain and wall elongation developed throughout loading history. It can be observed that even under axial load ratio of 0.05, except for initial minor compressive strains, the strain at this region of the wall is tensile throughout the loading, confirming that the axial load carrying capacity at this region is provided by the reinforcement only.

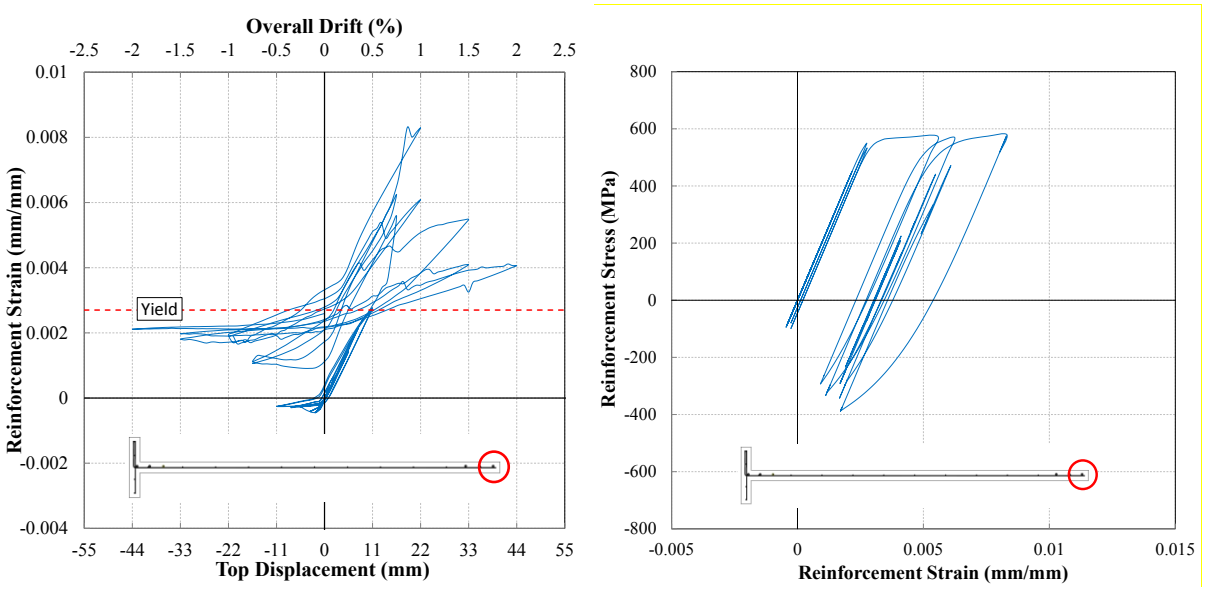

(a) (b)

Fig. 27 Response of the longitudinal reinforcement at the section exhibiting maximum out-of-plane deformation, TW1-a: (a) strain history; (b) stress-strain curve

3.6 TW1-b

In order to investigate the effect of axial load ratio on response of the wall, even in the case of lower shear span ratio 0.8, this model was analysed with no axial load. Being a squat wall, the model had considerable shear deformations. However, the lateral load-top displacement response (Fig. 28a) does

not show considerable degradation due to shear failure pattern which was observed in TW1-a. Instability of this model was due to the considerable out-of-plane deformation at the south boundary region as shown in Fig. 28b. The out-of-plane deformation increased by five times between 1.0 and 1.5% drift levels showing instability of the model. The out-of-plane displacement of this model is about ten times that of TW1-a, showing the effect of axial load ratio on response of the wall. The von Mises stress distribution (Fig. 29a) shows a diagonal strut as the only load carrying path since there is no axial load applied to the model. Fig. 29b displays a considerable out-of-plane deformation of the model, almost two times the lateral displacement at the corresponding drift level (1.5% drift). Fig. 30a shows the strain history of the south end region reinforcement at the section undergoing the maximum out-of-plane deformation. As can be seen in the figure, a significant residual tensile strain (about 0.0045) developed in the reinforcement during the 0.75% drift cycles, and consequently the cracks remained wide open forcing the bars to resist all vertical stresses, thereby resulting in considerable increase of the out-of-plane deformations. This residual strain increased significantly in the subsequent cycles and reached 0.01 during the 1.5% cycle before abrupt increase of the out of plane deformation and instability of the wall. Fig. 30a shows the maximum strain reached by the reinforcement at this drift level was ε_{sm}= 0.0136.

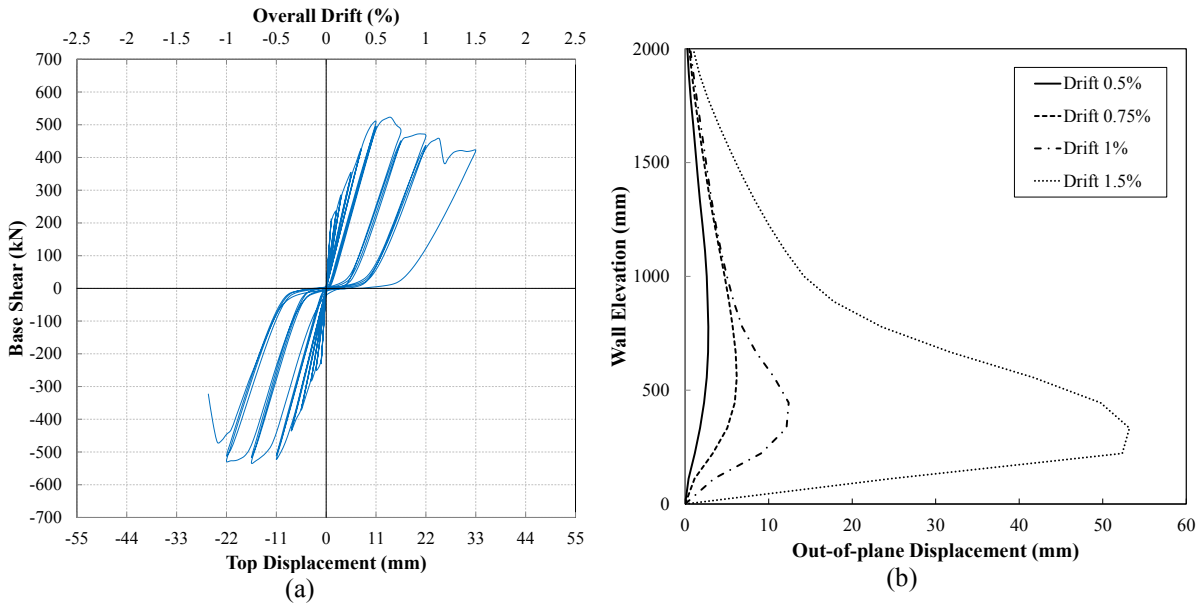

Fig. 28 Model response, TW1-b: (a) lateral load vs top displacement response; (b) maximum out-of-plane deformation corresponding to each drift level

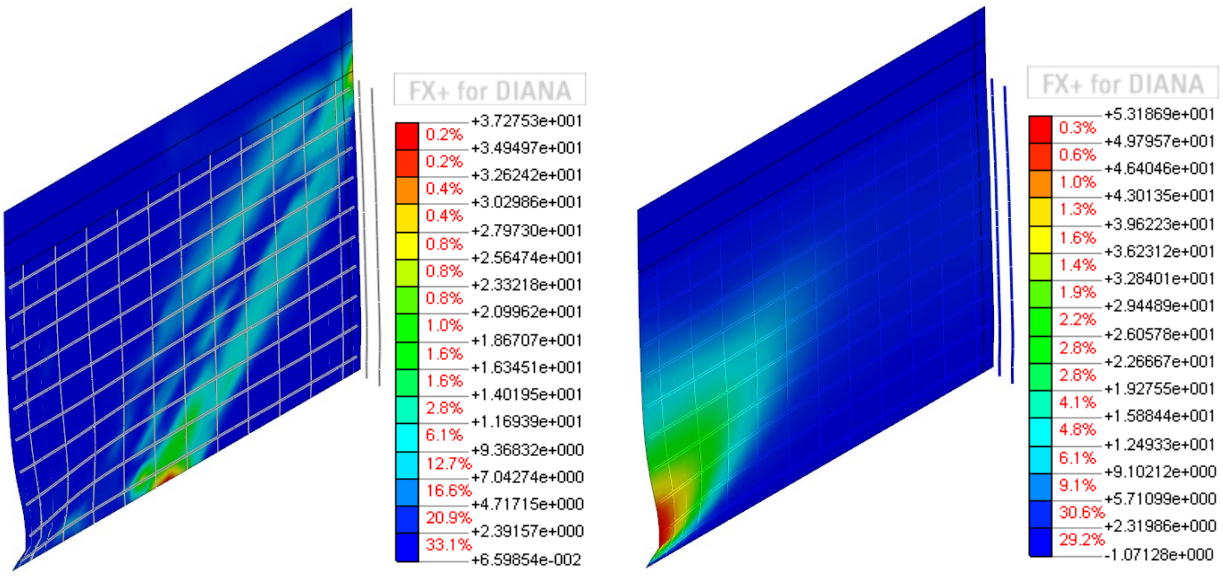

(a) (b)

Fig. 29 Model response at -1.5% drift, TW1-b: (a) von Mises stress distribution (MPa); (b) out-of-plane deformation (mm)

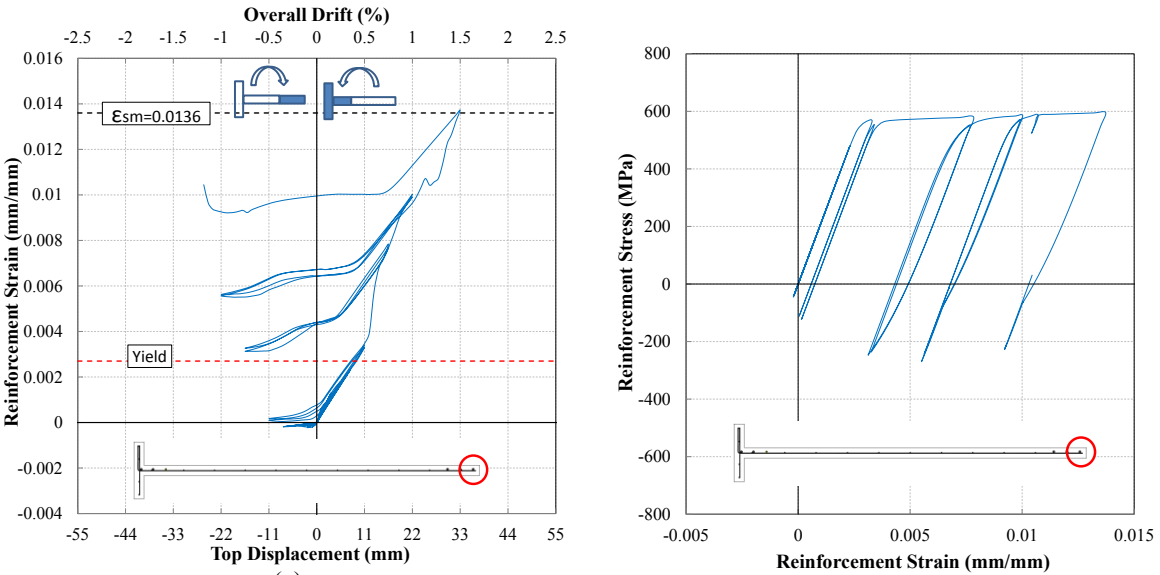

(a) (b)

Fig. 30 Response of the longitudinal reinforcement at the section exhibiting maximum out-of-plane deformation, TW1-b: (a) strain history; (b) stress-strain curve

3.7 TW1-c

In this section, the effect of reinforcement eccentricity on development of the out-of-plane deformation of the squat wall model is evaluated. For this purpose, the longitudinal and horizontal reinforcement elements are positioned at the section centreline, to represent the ideal condition of no eccentricity. Significant shear degradation is observed in this model as well (Fig. 31a). The out of plane mechanism is still triggered but the out-of-plane deformations are decreased by almost 35% when compared to the equivalent model with eccentricity TW1-a. The other response features (Fig. 32 and Fig. 33) resemble the ones of TW1-a, and are not hence described in this section.

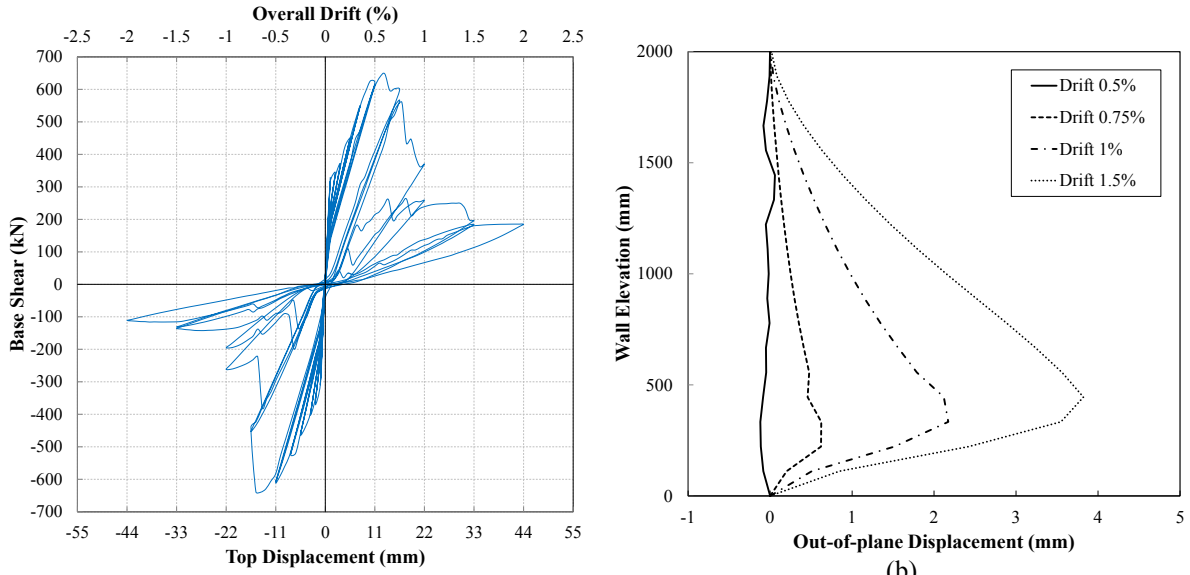

Fig. 31 Model response, TW1-c: (a) lateral load vs top displacement response; (b) maximum out-of-plane deformation corresponding to each drift level

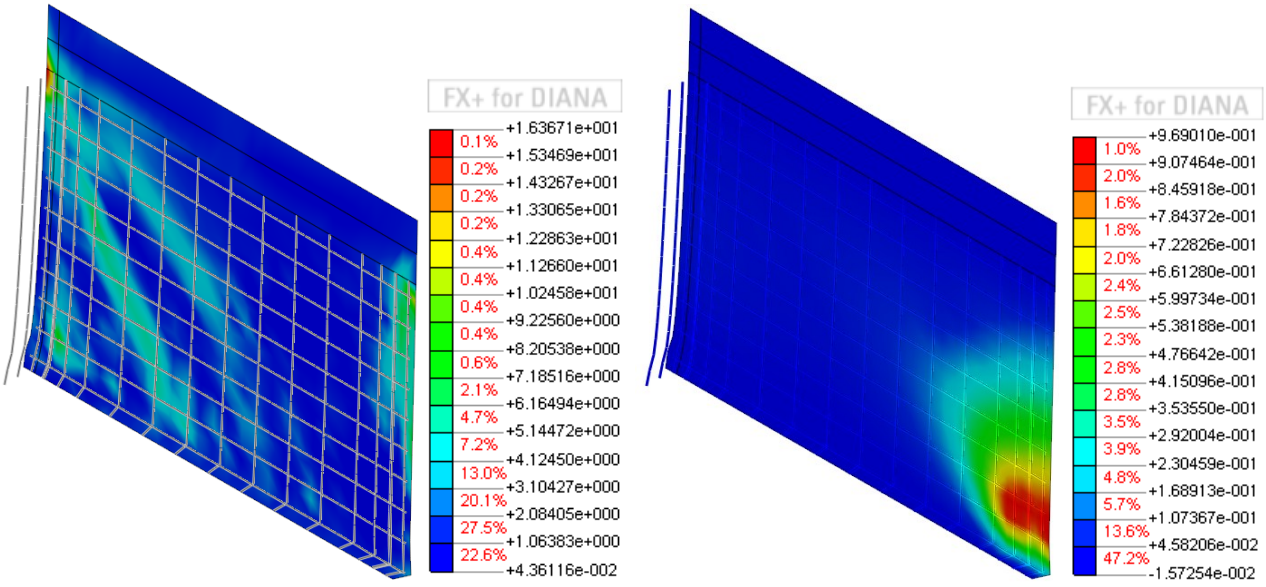

Fig. 32 Model response at -1.5% drift, TW1-c: (a) von Mises stress distribution; (b) out-of-plane deformation

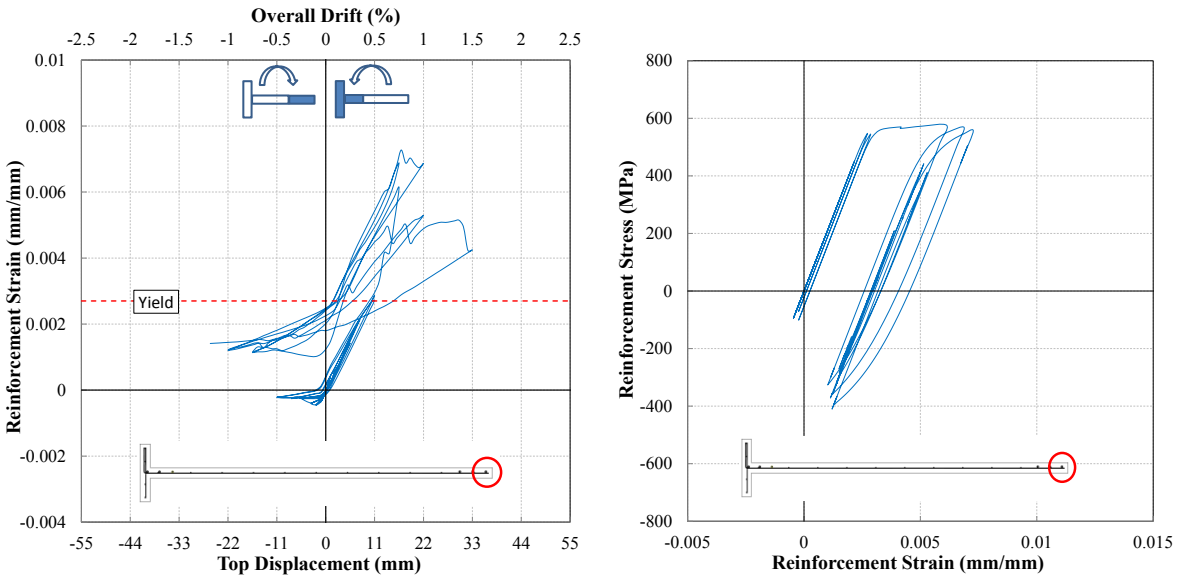

Fig. 33 Response of the longitudinal reinforcement at the section exhibiting maximum out-of-plane deformation, TW1-c: (a) strain history; (b) stress-strain curve

3.8 TW1-d

The squat wall model with no eccentricity is analyzed without axial load in this section. The lateral load versus top displacement response of the wall shows a considerable degradation during the 1.5% drift cycle (Fig. 34). However, despite having no eccentricity, the out-of-plane deformation is considerably large when compared to TW1-c, showing that the reduction of axial load ratio influences the response of this wall more than the eccentricity. The out-of-plane displacement of this model at 1.5% drift level is about 60% of that of TW1-b, showing that even a minor eccentricity, inevitable in construction particularly in singly reinforced walls, can significantly amplify out-of-plane deformations leading to instability and wall failure, as was observed in TW1-b. Fig. 36a shows the level of strain reached by the end region reinforcement of TW1-d before development of a considerable out-of-plane deformation. The level of this strain is almost identical to the one in TW1-b although the out-of-plane displacement is considerably lower at 1.5% drift level (33 mm compared to 53 mm) as no eccentricity was introduced in this case. Fig. 37 displays the maximum out-of-plane displacement of TW1-b and TW1-d throughout the loading. As can be seen in this figure, out-of-plane displacement of TW1-d recovered completely at lower drift levels until the 1.5% drift cycles, after which the out-of-plane displacement increased steadily and recovered only slightly. However, in the model with reinforcement eccentricity (i.e. TW1-b), the out-of-plane displacement did not recover during unloading from the 0.75% and 1.0% drift cycles, but its value was not large enough to make the wall unstable. During the 1.5% drift cycle, the out-of-plane displacement of TW1-b increased quite significantly resulting in wall instability.

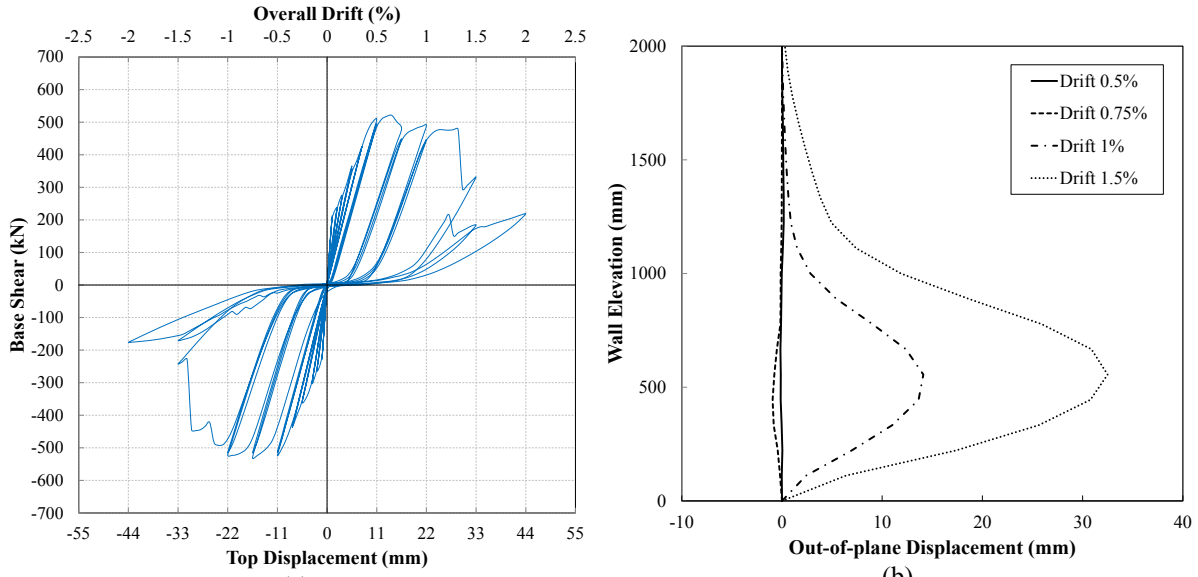

Fig. 34 Model response, TW1-d: (a) lateral load vs top displacement response; (b) maximum out-of-plane deformation corresponding to each drift level

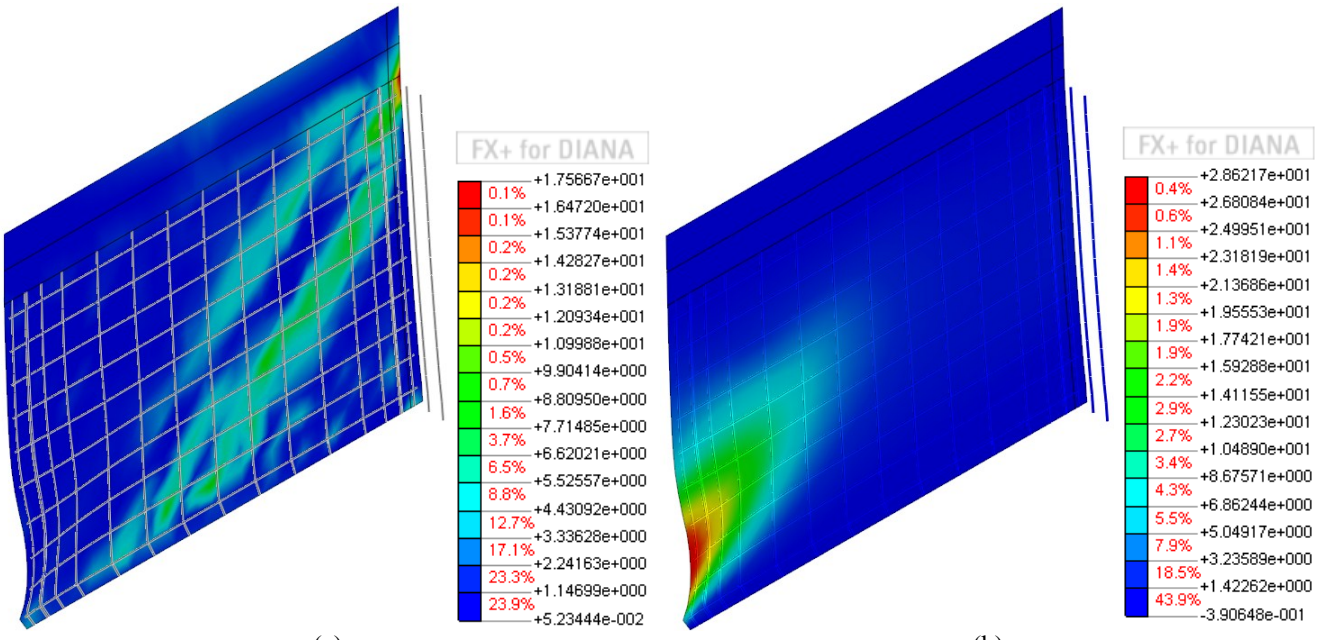

Fig. 35 Model response at -1.5% drift, TW1-d: (a) von Mises stress distribution; (b) out-of-plane deformation

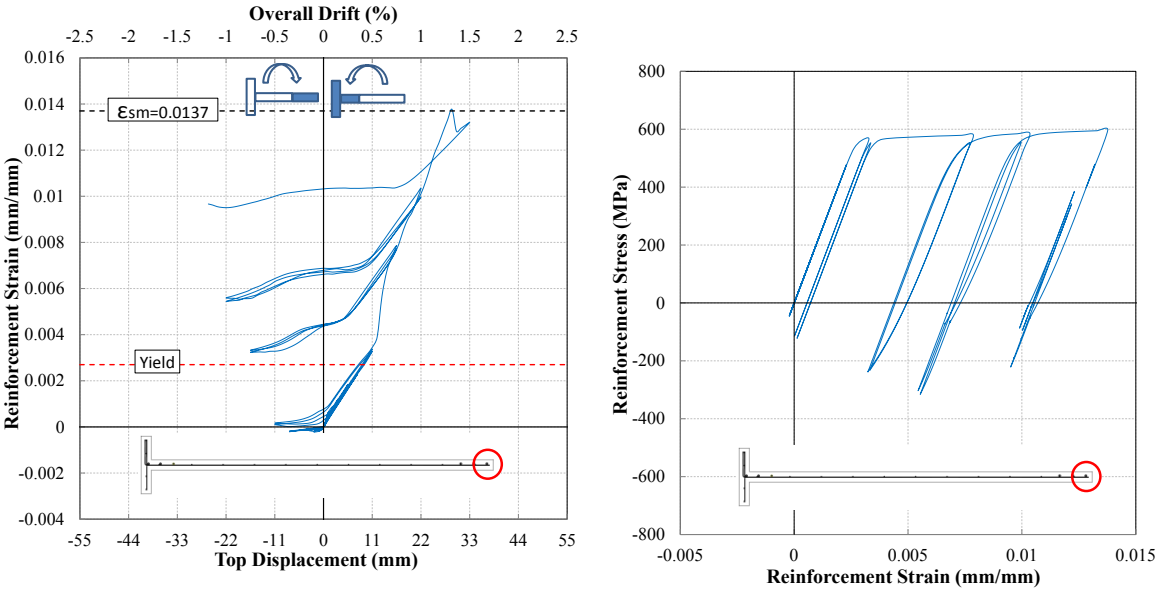

Fig. 36 Response of the longitudinal reinforcement at the section exhibiting maximum out-of-plane deformation, TW1-d: (a) strain history; (b) stress-strain curve

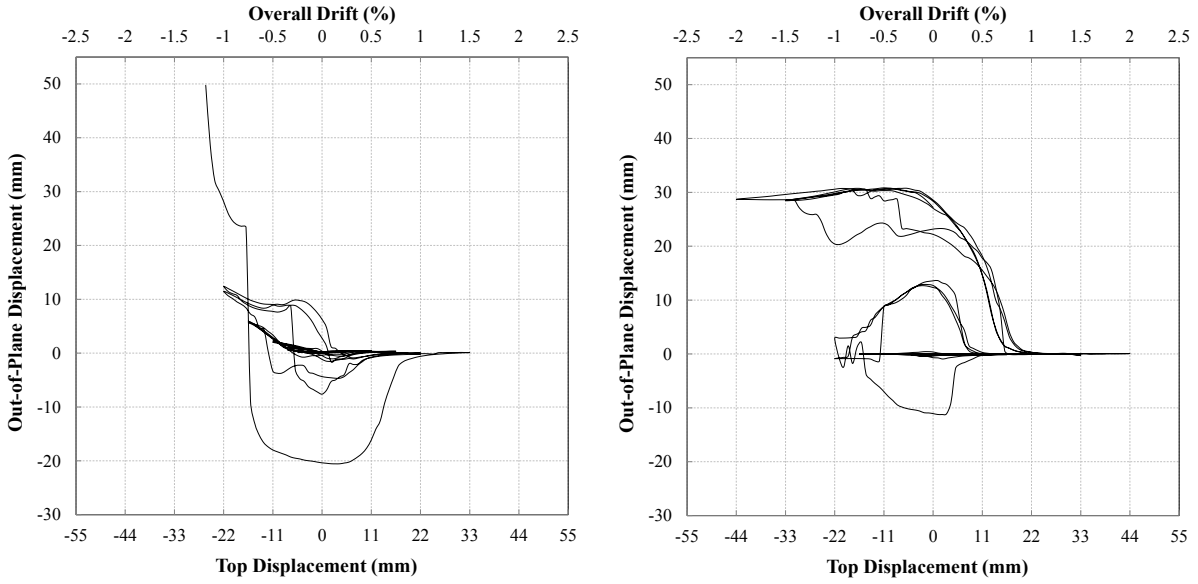

Fig. 37 Out-of-plane displacement history at 450 mm from the base: (a) TW1-b; (b) TW1-d

3.9 Discussion

The numerical investigation presented in this paper attempted to predict the failure patterns of a thin RC wall (TW1) tested in École Polytechnique Fédérale De Lausanne, Switzerland. Despite a short height of the specimen, the loading pattern was designed to represent a shear span of 10. For this purpose, in addition to the lateral displacement and axial load, a moment was also applied at the top of the specimen. Being a singly reinforced wall, the eccentricity of longitudinal reinforcement with respect to the loading plane could influence the out-of-plane deformation pattern. The model was

analyzed considering this effect as well as the effect of axial load which can also substantially affect the wall response. Another set of analysis was carried out by assuming a considerably lower shear-span ratio to investigate the effect of the same parameters in shear-dominated walls.

Fig. 38 shows the effect of axial load ratio on the slender test model (shear-span ratio = 3.7) and the squat wall loading configuration (shear-span ratio = 0.8). Comparison between Fig. 38a and Fig. 38b displays the rather significant shear degradation of the squat wall. The slender model had out-of-plane instability as a governing failure pattern as shown by the degradation in negative displacement zone of the cyclic response curve (Fig. 38a). According to Fig. 38b, although the lack of the axial load reduced the brittleness of the shear failure of the model, the out-of-plane deformation increased significantly, leading to an abrupt instability to the numerical model and preventing it from reaching 1.5% drift level. The larger out-of-plane displacements of the wall with no axial load are due to the development of large residual tensile strains in the longitudinal reinforcement at the end region which delays or prevent the closing of the crack requiring compressive load (due to bending) to be transferred only to the steel reinforcement in the cracked section. Out-of-plane instability of the slender as well as the squat model indicated that, regardless of the shear-span ratio, geometric configuration of wall sections such as its thickness could also render the wall prone to out-of-plane instability. Development of out-of-plane instability in rectangular walls and the governing parameters are studied by the authors in another study (Dashti et al. 2015).

The effect of reinforcement eccentricity on the slender wall was negligible although the eccentricity resulted in minor out-of-plane displacement at initial stages of loading. However, for the squat wall with no axial load the eccentricity resulted in earlier out-of-plane instability (Fig. 39). Development of out-of-plane displacement in these models (Fig. 16b and Fig. 22b) indicate that, up to 1% drift level, the out-of-plane displacement of both models is almost identical. However, the reinforcement eccentricity of TW1-A resulted in faster increase of the out-of-plane displacement leading to instability of the model (Fig. 39). This instability happened before compression crushing along the diagonal strut or yielding of shear reinforcement could result in a considerable strength degradation. Only the reinforcement "design" eccentricity based on the CAD drawings provided by the experimenters are considered in this study. However, in real construction practice, there can be additional sources of eccentricities depending on the construction accuracy such as eccentricity in wall thickness along the height or even concrete homogeneity along the height or thickness depending on the casting type, i.e. horizontal or vertical, which can significantly affect the wall response and generate bigger out-of-plane displacements at lower drift levels. The maximum reinforcement strain and maximum drift level reached by the south end region reinforcement

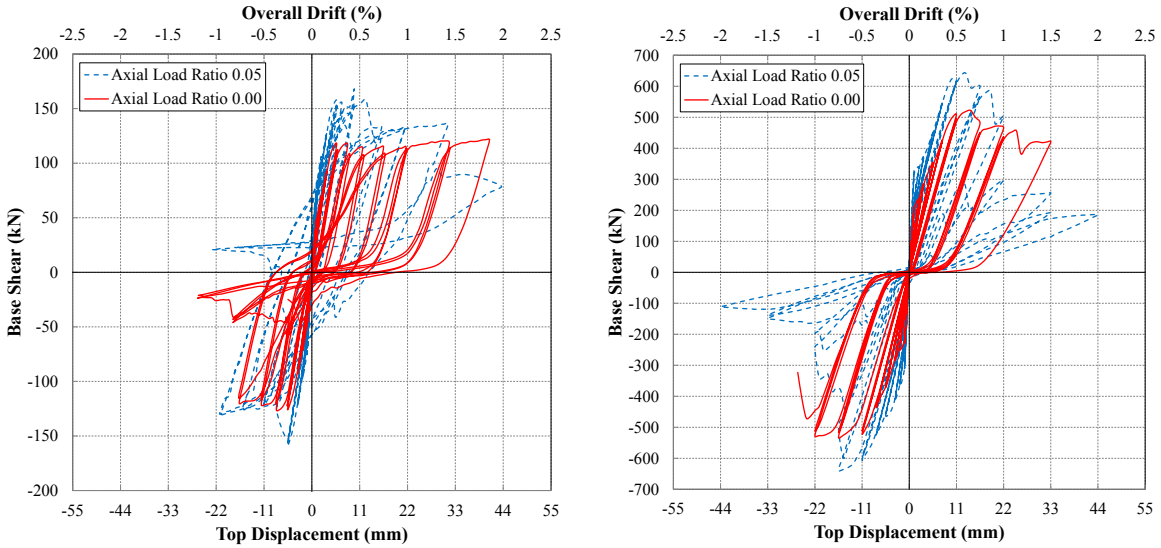

Fig. 38 Effect of axial load ratio: (a) shear-span ratio = 3.7; (b) shear-span ratio = 0.8

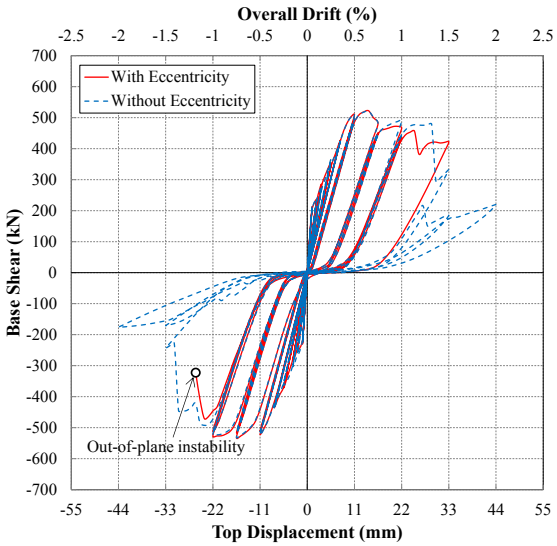

Fig. 39 Effect of reinforcement eccentricity

Table 2 compares the maximum tensile strain of extreme end reinforcement prior to initiation of out-of-plane deformation and initiation of out-of-plane instability as well as the corresponding drift cycles for different models. Initiation of out-of-plane deformation corresponds to the phase when the first out-of-plane deformation started and fully recovered. Initiation of out-of-plane instability refers to the phase when the out-of-plane deformation reached a considerably large value (generally greater than half of the wall thickness) and did not recover and increased steadily leading to instability of the wall model.

As can be seen in Table 2, TW1-A exhibited the initial out-of-plane deformation during the 0.50% drift cycle with the maximum reinforcement strain of 0.0053 (2.0εy) and became unstable during the 1.5% drift cycle with the maximum reinforcement strain of εsm = 0.0204 (7.6εy). When the axial load

was removed from the same model (TW1-B), the initial out-of-plane deformation occurred during the 0.50% drift cycle when the reinforcement strain reached 0.0072 (2.7εy) and the out-of-plane instability happened during the 1.0% drift cycle when the maximum reinforcement strain was 0.0169 (6.3εy). TW1-A had a lower reinforcement strain (0.015) at the same (1.0%) drift level which prevented the instability during this cycle. However, the end region reinforcement had to reach a significantly higher level of strain in the next drift level (0.0204 at 1.5% drift) which exceeded the critical value and provoked the wall instability.

The initial out-of-plane displacement of TW1-B (during the 0.50% drift) was about half of the corresponding value in TW1-A. However, the removal of axial load resulted in significantly faster growth of out-of-plane displacement in TW1-B compared to TW1-A, and caused a maximum out-of-plane displacement of about four times greater during the 1.0% drift cycle. The comparison between Fig. 15 and Fig. 18 indicates the effect of axial load on the strain history of the end bar. Although removal of axial load resulted in higher values of strain at peak drift levels, its effect on the values of strain during unloading/reloading phase and at around 0.0% drift level was greater. The difference in strain histories during the 0.75% and 1.0% drift cycles of TW1-A (Fig. 15) with the corresponding cycles of TW1-B (Fig. 18) is a good case in point. The zone around 0.0% drift level during unloading/reloading phase corresponds to development of the maximum out-of-plane deformation, and any variation in the residual tensile strain at this stage would considerably affect the possibility of timely crack closure and consequently out-of-plane response of the wall.

When eccentricity of the longitudinal reinforcement was removed from the model, i.e. TW1-C and TW1-D, the value of maximum strain in TW1-C and TW1-D at 1.0% drift increased to 0.0162 and 0.018, respectively. Both models became unstable at this drift level indicating that the critical strain value for this model could be around 0.016. The axial load ratio of TW1-D was 0.0 and understandably had a larger reinforcement strain compared to TW1-C. Also, the initial out-of-plane deformation happened at a later stage in TW1-C ($\varepsilon_{sm} = 0.01$ during the 0.75% drift cycle) compared to TW1-A, and occurred at the same drift cycle in TW1-D as TW1-B.

The effect of eccentricity in position of the longitudinal reinforcement with respect to the loading plane was observed in the models with low shear-span ratios, as well. As can be seen in Table 2, removal of this eccentricity resulted in a delay in initiation of out-of-plane deformation and consequently caused the corresponding values of reinforcement strain to be higher by more than two times. Among the models with low shear-span ratios, only TW1-b and TW1-d that had no axial loads exhibited out-of-plane instabilities. The values of ε_{sm} and drift levels corresponding to instability phase were identical for these models but TW1-b was eccentrically reinforced and, as discussed above, exhibited faster increase of out-of-plane displacement.

Use of a single layer of reinforcement makes structural walls more susceptible to out-of-plane instability failure. This is because following the development of large tensile residual strains in the

longitudinal reinforcement, a single layer of vertical reinforcement lacks a ability to restore stability when of the bars yield in compression before crack closure can the previously cracked concrete to compressive stress. In doubly reinforced sections, this instability can be delayed as both layers of longitudinal reinforcement would not undergo identical amounts of tensile and compressive strains due to the inherent eccentricities of the wall section along its thickness, and the second layer of longitudinal reinforcement would help restore stability of the section if only one of the layers yielded in compression.

Table 2 Reinforcement strain and drift levels prior to initiation of out-of-plane instability

Model	Shear-Span Ratio	Eccentricity	Axial Load Ratio	OOP Deformation		OOP Instability	
				ε_{sm}	Drift	ε_{sm}	Drift
TW1- A	3.7	Yes	0.05	0.0053 ($2.0\varepsilon_y$)	0.50%	0.0204 ($7.6\varepsilon_y$)	1.5%*
TW1- B	3.7	Yes	0.00	0.0072 ($2.7\varepsilon_y$)	0.50%	0.0169 ($6.3\varepsilon_y$)	1.0%
TW1- C	3.7	No	0.05	0.01 ($3.7\varepsilon_y$)	0.75%	0.0162 ($6.0\varepsilon_y$)	1.0%
TW1- D	3.7	No	0.00	0.008 ($3.0\varepsilon_y$)	0.50%	0.018 ($6.7\varepsilon_y$)	1.0%
TW1- a	0.8	Yes	0.05	0.0027 ($1.0\varepsilon_y$)	0.50%	NA	NA
TW1- b	0.8	Yes	0.00	0.0033 ($1.2\varepsilon_y$)	0.50%	0.0136 ($5.0\varepsilon_y$)	1.5%
TW1- c	0.8	No	0.05	0.006 ($2.2\varepsilon_y$)	0.75%	NA	NA
TW1- d	0.8	No	0.00	0.008 ($3.0\varepsilon_y$)	0.75%	0.0137 ($5.0\varepsilon_y$)	1.5%

Note: ε_{sm} = Maximum tensile strain of extreme end reinforcement prior to initiation of out-of-plane deformation/instability; Drift = maximum in-plane drift level of the specimen prior to initiation of out-of-plane deformation/instability.
*At 1.0% drift level, the maximum tensile strain of extreme end reinforcement in TW1-A was 0.015 (arguably just below the critical strain ~ 0.016).

4 Prediction vs. Experimental comparison

Fig. 40 compares the numerical model predictions with the experimental observations reported by Rosso et al. (2015) and Almeida et al. (2017). As can be seen in Fig. 8, the model was loaded up to 2% drift level before being terminated due to numerical instability. For the sake of better comparison between experimental and predicted load-displacement curves, Fig. 40a does not display the numerical model results beyond the 1.5% drift cycle. During this cycle and upon unloading of the model, a significantly large out-of-plane displacement occurred (Point c, Fig. 8), which increased steadily up to reloading in the reverse direction (Fig. 11b).

The in-plane load-displacement response of the tested specimen (shown in Fig. 40a) displays a reasonable agreement with the analytically predicted response. However, the drop of strength does not seem to be well captured by the model. According to the parametric studies described in the previous sections (Sections 3-1 to 3-8), this abrupt drop of strength were predicted in other wall models that were subjected to axial load ratio of 0.05.

As a mesh sensitivity analysis was not carried out and a relatively fine mesh was adopted to capture a better prediction of the out-of-plane displacement pattern along the wall height, localization of deformations was inevitable. In order to further investigate this effect, the tested wall is modelled and analyzed here again (as a controlled modification to the blind predictions) with medium and coarse mesh configurations. Fig. 41 displays the effect of mesh size on the monotonic response of the

model. As can be seen in this figure, the increase in mesh size has resulted in delay of the strength drop. Localization in finite element analysis has been thoroughly studied by Bažant and Oh (1983), Bazant and Planas (1997) and De Borst (1997), and the concrete post-peak tensile stress-strain response model as well as concrete compressive response are generally regularized to limit mesh sensitivity. In this prediction, the material model regularization was not addressed.

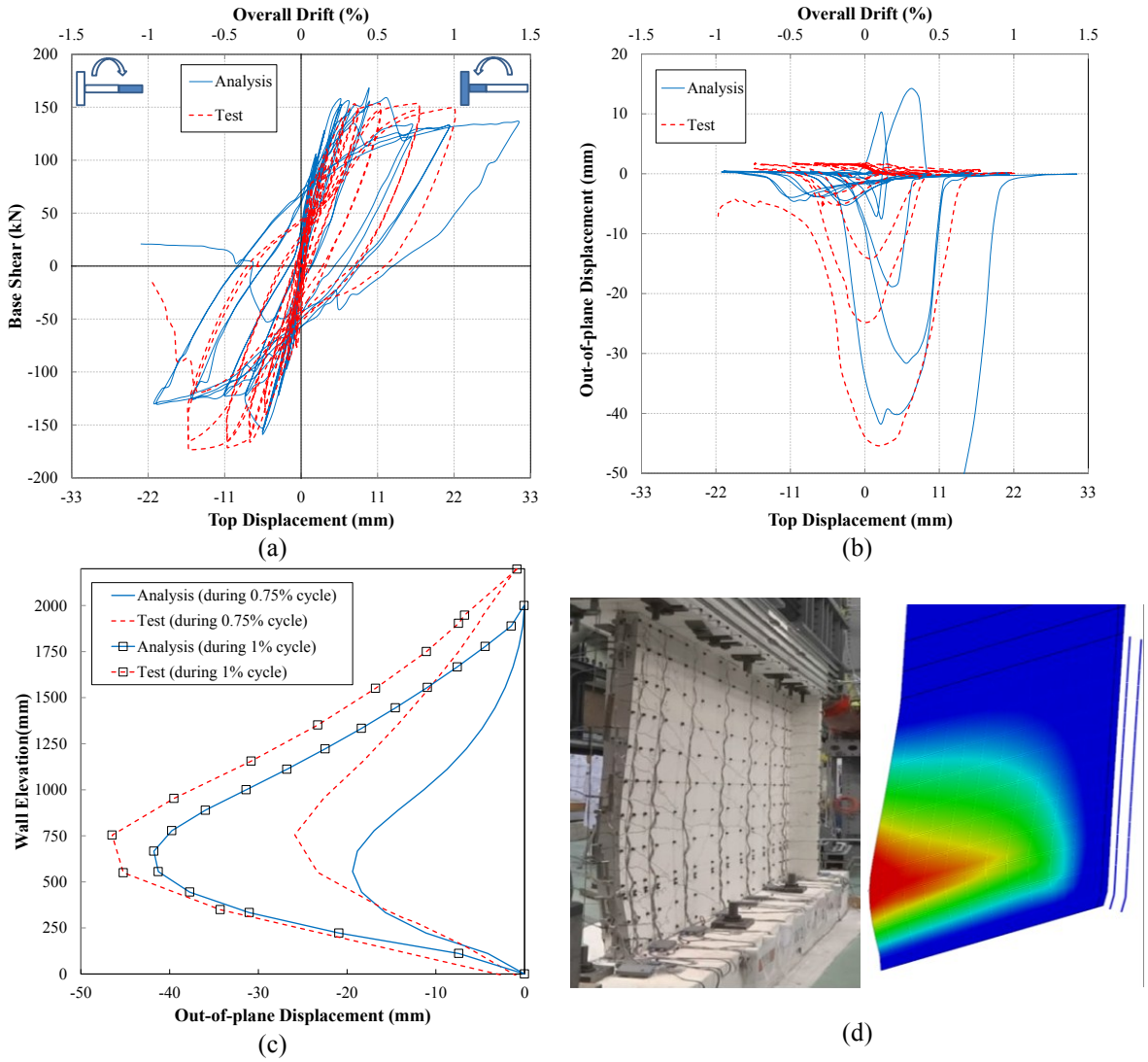

Fig. 40 Verification of the blind prediction: (a) in-plane load-displacement response of the wall; (b) in-plane vs out-of-plane displacement response of the wall; (c) out-of-plane displacement profile along the wall height; (d) experimental observation vs numerical simulation of out-of-plane deformation, photo courtesy of Rosso et al. (2015)

Fig. 40b displays the maximum out-of-plane displacement of the wall at different stages of loading. As can be seen in this figure, the numerical model could reasonably predict the development of the out-of-plane deformation. In both numerical prediction and test results, the out-of-plane displacement initiated at small drift levels, and increased along with increase of the drift level. At every cycle, out-of-plane displacement initiated and increased when unloading from the peak displacement of the cycle and recovered when reloading in the reverse direction. This phenomenon

well describes dependency of the out-of-plane deformation of a wall section on the residual strain of the reinforcement and the crack opening corresponding to the peak in-plane displacement of a specific cycle. The numerical model could reasonably predict the milestones of the out-of-plane displacement; particularly the points corresponding to the maximum out-of-plane displacement.

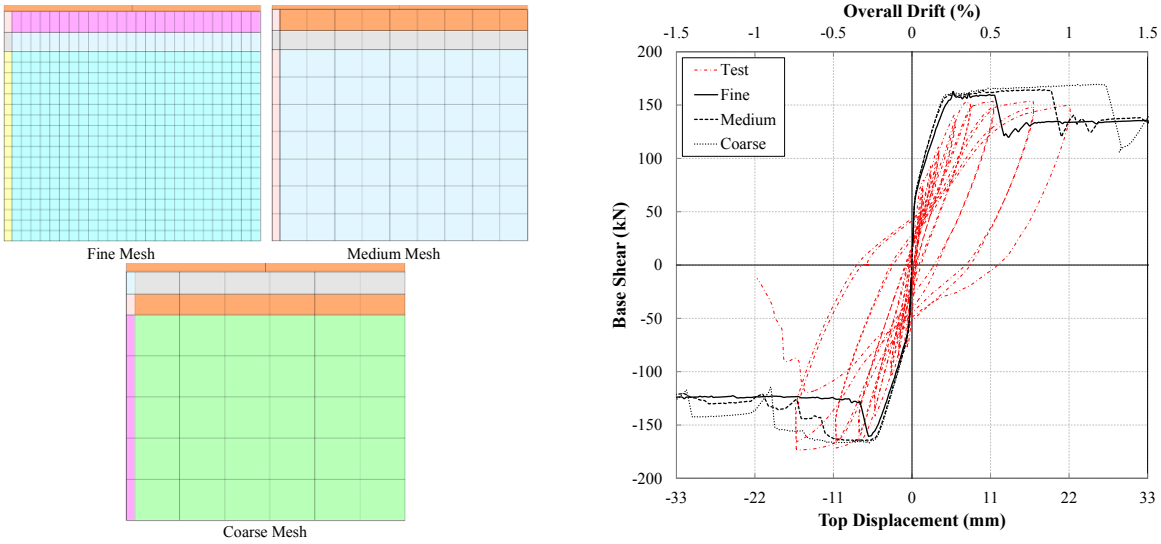

Fig. 41 Sensitivity of the model to mesh size

Fig. 40c shows the maximum out-of-plane displacement profile along the wall height predicted by the model in comparison with the experimental observations. The wall height corresponding to the maximum out-of-plane displacement was reasonably predicted by the model. However, due to the representation of the cap beam and the extended height of the model (Fig. 6) using linear elastic material properties (to simulate the shear-span ratio experimentally adopted in the loading regime) the value of the out-of-plane displacement is zero above the 2000 mm elevation of the wall, while the test measurements display non-zero values for this zone. Fig. 40d compares the out-of-plane deformation pattern of the specimen with the numerical simulation.

5 Conclusion

The capability of a numerical model developed to simulate the out-of-plane displacement of rectangular structural walls subjected to in-plane loading was further verified through blind prediction of the response of a wall specimen tested in École Polytechnique Fédérale de Lausanne (EPFL). The specimen was a singly reinforced T-shaped wall panel with a shear-span ratio of 3.7 and subjected to uni-directional (in-plane) quasi-static reversed cyclic loading regime.

The numerical model could predict the lateral load-top displacement response of the specimen reasonably well and exhibited a flexure-dominated response accompanied by out-of-plane

deformations. The out-of-plane displacement of the specimen at different drift levels was well captured by the model. Furthermore, the model could simulate the out-of-plane instability of the specimen, which was characterized by an abrupt degradation of the cyclic load displacement curves.
A parametric analysis was carried out addressing the effects of axial load ratio, shear-span ratio, and eccentricity of the longitudinal bars on response of the specimen.

The axial load proved to affect the development of out-of-plane deformation in rectangular walls by controlling the values of strain developed in the longitudinal reinforcement at different stages of a specific cycle. This effect was significantly large during unloading/reloading phase and at around 0.0% drift level in a loading cycle, which is the stage corresponding to the maximum out-of-plane displacement.

Out-of-plane deformation of the slender as well as the squat wall models indicated that, regardless of the shear-span ratio, geometric configuration of wall sections such as its thickness could also render the wall prone to out-of-plane instability. The maximum tensile strain corresponding to initiation of out-of-plane deformation and out-of-plane instability was lower in squat wall models when compared to the slender ones.

Being a singly reinforced wall, the eccentricity of longitudinal reinforcement with respect to the loading plane influenced the out-of-plane response and resulted in its earlier initiation. However, its effect during the final stages of the wall response and formation of out-of-plane instability was not very significant.

Since accumulation of residual tensile strain in bars under cyclic loading leads to a significant delay in crack closure and all compression is taken by the bars at this stage, the wall is prone to undergo out-of-plane deformations in the compression boundary region if yielding in compression occurs before crack closure. Therefore, depending on the initial tensile strain developed in the longitudinal reinforcement, different scenarios can happen. If this strain is less than a critical value, timely crack closure can activate contribution of concrete to the load-carrying capacity of the section and lead to recovery of any out-of-plane deformation that had taken place. Otherwise, the out-of-plane deformation can increase steadily and lead to out-of-plane instability of the wall. Based on the numerical model predictions and the parametric studies, this critical value of strain could be around six times the yield strain for the tested specimen.

6 Acknowledgment

The authors wish to acknowledge Prof. Katrin Bayer and her research team at EPFL (Joa˜o P. Almeida and Angelica Rosso) for providing the input data of their experimental tests and facilitating the predictions.

Also, the financial support provided by the Ministry of Business, Innovation and Employment (MBIE), SAFER concrete project and the Quake Centre at University of Canterbury to conduct this research is greatly acknowledged.

7 REFERENCES

Almeida J, Prodan O, Rosso A, Beyer K (2017) Tests on Thin Reinforced Concrete Walls Subjected to In-plane and Out-of-plane Cyclic Loading Earthquake Spectra 33:323-345

Bažant ZP, Oh BH (1983) Crack band theory for fracture of concrete Matériaux et construction 16:155-177

Bazant ZP, Planas J (1997) Fracture and size effect in concrete and other quasibrittle materials vol 16. CRC press,

Beattie GJ (2004) Design of Slender Precast Concrete Wall Panels – Experimental Testing. BRANZ Ltd, Judgeford, New Zealand, BRANZ Study Report SR 129

Chai YH, Elayer DT (1999) Lateral stability of reinforced concrete columns under axial reversed cyclic tension and compression ACI Structural Journal 96:780-789

Dashti F, Dhakal R, Pampanin S Development of out-of-plane instability in rectangular RC structural walls In: 2015 NZSEE Conference, Rotorua, New Zealand, 2015. New Zealand Society for Earthquake Engineering,

Dashti F, Dhakal RP, Pampanin S (2014) Blind prediction of a thin RC wall (TW1) tested in École Polytechnique Fédérale de Lausanne. Personal Communication, University of Canterbury

Dashti F, Dhakal RP, Pampanin S (2017a) Numerical Modeling of Rectangular Reinforced Concrete Structural Walls Journal of Structural Engineering 143 doi:doi:10.1061/(ASCE)ST.1943-541X.0001729

Dashti F, Dhakal RP, Pampanin S (2017b) Validation of a Numerical Model for Prediction of Out-of-plane Instability in Ductile Structural Walls under Concentric In-plane Cyclic Loading (revised manuscript under review) Journal of Structural Engineering

De Borst R (1997) Some recent developments in computational modelling of concrete fracture International journal of fracture 86:5-36

DIANA T (2011) Finite Element Analysis User's Manual - Release 9.4.4, 9.4.4 edn. TNO DIANA,

Filippou FC, Popov EP, Bertero VV (1983) Effects of bond deterioration on hysteretic behavior of reinforced concrete joints

Goodsir WJ (1985) The design of coupled frame-wall structures for seismic actions. University of Canterbury

Johnson B (2010) Anchorage detailing effects on lateral deformation components of R/C shear walls. Master Thesis, University of Minnesota

Krolicki J, Maffei J, Calvi G (2011) Shear strength of reinforced concrete walls subjected to cyclic loading Journal of Earthquake Engineering 15:30-71

Mander J, Priestley MN, Park R (1988) Theoretical stress-strain model for confined concrete Journal of structural engineering 114:1804-1826

Menegotto M, Pinto P Method of Analysis for Cyclically Loaded Reinforced Concrete Plane Frames Including Changes in Geometry and Non-elastic Behavior of Elements Under Combined Normal Force and Bending. In: IABSE Symposium on the Resistance and

Ultimate Deformability of Structures Acted on by Well-Defined Repeated Loads, Lisbon, 1973. Association internationale des ponts et charpentes,
Mindlin RD (1951) Influence of rotary inertia and shear on flexural motions of isotropic, elastic plates J of Appl Mech 18:31-38
Moyer MJ, Kowalsky MJ (2003) Influence of tension strain on buckling of reinforcement in concrete columns ACI Structural Journal 100
Oesterle R (1979) Earthquake Resistant Structural Walls: Tests of Isolated Walls: Phase II. Construction Technology Laboratories, Portland Cement Association,
Paulay T, Priestley M (1993) Stability of ductile structural walls ACI Structural Journal 90:385-392
Reissner E (1945) The effect of transverse shear deformation on the bending of elastic plates Journal of applied Mechanics 12:69-77
Rosso A, Almeida J, Beyer K (2015) Stability of thin reinforced concrete walls under cyclic loads: state-of-the-art and new experimental findings Bull Earthquake Eng:1-30 doi:10.1007/s10518-015-9827-x
Rosso A, Almeida JP, Beyer K (2014) Short report on the experimental cyclic test of a thin RC wall (TW1) for blind prediction purposes. ÉCOLE POLYTECHNIQUE FÉDÉRALE DE LAUSANNE,
Thomsen IV JH, Wallace JW (2004) Displacement-based design of slender reinforced concrete structural walls-experimental verification Journal of structural engineering 130:618-630
Vallenas JM, Bertero VV, Popov EP (1979) Hysteretic behaviour of reinforced concrete structural walls. Earthquake Engineering Research Center, University of California, Berkeley.,
Vecchio FJ, Collins MP (1986) The modified compression-field theory for reinforced concrete elements subjected to shear ACI Journal Proceedings 83:219-231